

THE INVESTIGATION OF INTERFACES OF  
MULTILAYER MULTIAXIS FIBER  
REINFORCED COMPOSITES BY FIBER  
BRAGG GRATING SENSORS

by

Ataman Deniz

**Submitted to**  
**the Graduate School of Engineering and Natural Sciences**  
**in partial fulfillment of**  
**the requirements for the degree of**  
**Master of Science**

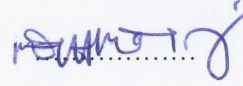
**SABANCI UNIVERSITY**

September 2014

THE INVESTIGATION OF INTERFACES OF  
MULTILAYER MULTIAxis FIBER  
REINFORCED COMPOSITES BY FIBER  
BRAGG GRATING SENSORS

APPROVED BY:

Assoc. Prof. Dr. Mehmet Yıldız  
(Thesis Supervisor)



Assoc. Prof. Dr. Bahattin Koç



Assoc. Prof. Dr. Burç Mısırlıođlu



DATE OF APPROVAL: 06/08/14

© Ataman Deniz 2014

All Rights Reserved

The Investigation of Interfaces of Multilayer Multiaxis Fiber Reinforced Composites by  
Fiber Bragg Grating Sensors

Ataman Deniz

MAT, M.Sc. Thesis, 2014

Thesis Supervisor: Assoc. Prof. Dr. Mehmet Yıldız

**Keywords:** *structural health monitoring (SHM), fiber Bragg gratings (FBG), interply hybrid composites, resin transfer molding (RTM)*

**Abstract**

Advanced Composites, due to their high strength to weight ratio, replaced conventional materials in many applications. The role of structural health monitoring (SHM) in development of advanced composites is proved by many in industry and academia. In this thesis work, vacuum infusion and resin transfer molding (RTM) were developed for advanced composite production. Within the context of advanced composite development project, a fully functioning mechanical test laboratory is built in Yonca-Onuk JV shipyard and also fundamental composite configurations were subjected to mechanical tests. In the last stage, interply hybrid composite configurations that can be used for advanced composites were tested with embedded fiber Bragg grating (FBG) sensors.

Çok Ensenli Fiber Oryantasyonuna Sahip Çok Katmanlı Kompozit Malzemelerinin  
Arayüzlerindeki Mekanik Davranışların Fiber Bragg Sensörlerle İzlenmesi

Ataman Deniz

MAT, M.Sc. Tez, 2014

Tez Danışmanı: Doç. Dr. Mehmet Yıldız

**Anahtar Kelimeler:** *yapısal sağlık gözetimi (SHM), fiber Bragg ızgara (FBG), katmanlar arası hibrit kompozitler, reçine kalıplama (RTM)*

### Özet

İleri kompozit yapılar, spesifik mukavemetleri ve düşük özgül ağırlıkları gibi sebeplerden dolayı birçok mühendislik uygulamasında geleneksel metallerin yerini almıştır. Yapısal sağlık gözetimi (SHM) sistemlerinin, ileri kompozitlerin geliştirilmesindeki rolleri, daha önce yapılmış akademik ve endüstriyel çalışmalarla kanıtlanmıştır. Bu tez çalışmasında da, ileri kompozitlerin geliştirilmesinde kullanılabilen vakum infüzyon ve reçine kalıplama üretim metotları tasarlanmıştır. Son üründe kullanılacak kompozitlerin geliştirilmesi projesi kapsamında kullanılacak bir mekanik test laboratuvarı Yonca-Onuk Ltd. tersanesine kurulmuş ve yine bu proje kapsamında temel malzeme konfigürasyonları testleri gerçekleştirilmiştir. Daha sonrasında ileri kompozitlerin oluşturulmasında kullanılabilen katmanlar arası hibrit malzeme konfigürasyonları, gömülü fiber optik sistemlerle test edilmiş ve davranışları sunulmuştur.

To my family...

## ACKNOWLEDGEMENT

I would like to thank to

Professor Mehmet Yıldız for patiently guiding not just this thesis work but my engineering career as well

Jury members, Professor Bahattin Koç and Burç Mısırlıođlu for their time and highly valuable critics to make this thesis worth reading

Onuk Taşıt A.Ş. members, especially, Ekber Onuk, Hakan Çelik and İbrahim Günal for providing feedback and sharing their facilities

SANTEZ for funding my education for 1.5 years through the project 1307.STZ.2012-1

Professor Özgür Demircan for teaching me the way he did in Japan

SPH members, Amin Rahmat, Nima Tofighi and Murat Özbulut for answering my unending totally irrelevant questions

L010 folks, Çağatay Yılmaz, Çağdaş Akalın, Esat Selim Kocaman and Ece Belen for having meaning more than teammates

Fazlı Fatih Melemez and Pandian Chelliah for making the life in laboratory much more enjoyable

My two equally beautiful nieces for just being around and smiling

My parents, my brothers, my sisters in law and my fiancée for their limitless support

## Table of Contents

CHAPTER 1.....	1
Introduction.....	1
1.1. Motivation.....	1
1.2. Outline of the Thesis .....	3
CHAPTER 2.....	5
Literature Review.....	5
2.1. Hybrid Fiber Reinforced Composite.....	5
2.2. Fiber Bragg Gratings.....	8
2.3. Fiber Reinforced Composite Manufacturing Methods.....	12
CHAPTER 3.....	19
Fiber Reinforced Composite Manufacturing Method Design.....	19
3.1. Resin Transfer Mold Design .....	19
3.2. Vacuum Infusion Unit.....	28
CHAPTER 4.....	29
Experimental Composite Specimen Testing .....	29
4.1. Mechanical Analysis of Advanced Composites.....	29
4.2. The Investigation of Tensile Behavior of Interply Glass/Carbon Hybrid Composites by Fiber Bragg Gratings.....	33
CHAPTER 5.....	51
Conclusion .....	51
References .....	53

## List of Figures

<i>Figure 1.1: Product development stages</i> .....	1
<i>Figure 1.2: Strength of several type of engineering materials[3]</i> .....	2
<i>Figure 1.3: FBG sensor locations on a train carbody [4]</i> .....	3
<i>Figure 2.1: Schematic model of unidirectional carbon/glass fibers interply hybrid composite</i> .....	6
<i>Figure 2.2: Stress versus strain behavior with respect to CF to GF ratio</i> .....	7
<i>Figure 2.3: Optical fiber layers, a) the core, b) the cladding and c) protective layer</i> .....	8
<i>Figure 2.4: Fiber Bragg gratings</i> .....	10
<i>Figure 2.5: Microbending in optical fibers</i> .....	11
<i>Figure 2.6: FBG strain gradient sensitivity of strain gradient with respect to grating length [14]</i> .....	12
<i>Figure 2.7: Production and performance characteristics of several type of manufacturing methods [3]</i> .....	13
<i>Figure 2.8: Hand lay-up schematics [18]</i> .....	14
<i>Figure 2.9: Vacuum bagging [18]</i> .....	15
<i>Figure 2.10: Vacuum infusion [19]</i> .....	16
<i>Figure 2.11: Resin transfer molding, in some applications vents are vacuumed [19]...</i>	17
<i>Figure 2.12: Autoclave vessel [18]</i> .....	18
<i>Figure 3.1: Preceding RTM; rectangular glass is visible</i> .....	21
<i>Figure 3.2: Revised RTM; shape of the glass is similar to o-ring path</i> .....	22
<i>Figure 3.3: Render image of the new RTM</i> .....	23
<i>Figure 3.4: Important molding surface features</i> .....	24
<i>Figure 3.5: A flow path example</i> .....	25
<i>Figure 3.6: Load vectors</i> .....	26
<i>Figure 3.7: a) Moment as a function of cover angle, b) Lifting force required by operator at the particular angle</i> .....	26
<i>Figure 3.8: a) Mesh model of mold cover – gas spring connecting arm, b) Stress result</i> .....	27
<i>Figure 3.9: Loading results at cover hinges</i> .....	27

<i>Figure 3.10: a) prepreg manufacturing by vacuum infusion table, b) nanophase reinforced composite manufacturing</i> .....	28
<i>Figure 4.1: Composite development stages</i> .....	29
<i>Figure 4.2: Mechanical testing laboratory setup</i> .....	30
<i>Figure 4.3: a) An example chord modulus testing setup, b) specimens prior to the testing, c) specimens after the testing, notice the necking behavior</i> .....	32
<i>Figure 4.4: a) First test of transverse extensometer versus transverse strain gage, b) second test with same specimen</i> .....	33
<i>Figure 4.5: Reinforcements</i> .....	36
<i>Figure 4.6: Interrogator and L shaped specimen</i> .....	36
<i>Figure 4.7: A) FBG location, B) stitched optical fiber, C) optical fiber ingress location</i> .....	37
<i>Figure 4.8: Hybrid stacking sequences, green layers are carbon fiber, white layers are glass fiber reinforcements</i> .....	38
<i>Figure 4.9: Labview code for extensometer data acquisition</i> .....	39
<i>Figure 4.10: Testing setup</i> .....	39
<i>Figure 4.11: Stress strain curves of neat specimens</i> .....	41
<i>Figure 4.12: a) undamaged specimen, b) first ply splitting, c) complete failure of carbon fiber plies</i> .....	43
<i>Figure 4.13: Stress versus strain result of carbon fiber reinforced composite</i> .....	43
<i>Figure 4.14: a) Stress and strain curves of carbon only specimen with respect to test time, b) close-up curves</i> .....	44
<i>Figure 4.15: Stress and strain on double Y axis plot of glass fiber reinforced composite</i> .....	45
<i>Figure 4.16: a) stress and strain curves of hybrid 1, b) close-up curve, the location is demonstrated by dashed rectangle, c) Fx curve of hybrid 1, d) close-up Fx curve</i> .....	46
<i>Figure 4.17: a) stress and strain curves of hybrid 2, b) close-up curve, c) Fx curve of hybrid 2, d) close-up Fx curve</i> .....	47
<i>Figure 4.18: a) stress and strain curves of hybrid 1, b) close-up curve, c) Fx and Sx curves of hybrid 3, d) close-up Fx and Sx curve</i> .....	49

## List of Tables

<i>Table 4.1: Chord modulus results of the -45/+45° CF specimen.....</i>	<i>31</i>
<i>Table 4.2: Ultimate tensile stress results of -45/+45° CF specimen.....</i>	<i>32</i>
<i>Table 4.3: Properties of textile reinforcements .....</i>	<i>35</i>
<i>Table 4.4: Specimen Thickness (mm) .....</i>	<i>38</i>
<i>Table 4.5: Pm wavelength shift per 1 <math>\mu\epsilon</math> coefficient of specific FBG sensors.....</i>	<i>41</i>
<i>Table 4.6: Maximum recorded wavelength shift (nm) per specimen.....</i>	<i>50</i>

## CHAPTER 1

### Introduction

#### 1.1. Motivation

A high end composite part passes through 4 major stages, shown in the figure 1.1, during its development lifetime. The design stage intents to achieve a specific requirement and covers both the structural design and the material design. The structural design ranges from simple forms to complex shapes whereas the material design is the combination of available materials for achieving specific function. The production stage covers variety of manufacturing techniques in order to realize the structure. Within the context of the validation stage, virtual simulations and experimental tests would evaluate performance of the structure and the material. Last, structural health monitoring, unlike validation, focuses on observation of the structure under normal use throughout its lifetime. Initially these stages may seem independent from each other, however, for example, it would be unreasonable to design a part that is impossible to manufacture.



**Figure 1.1: Product development stages**

Within the context of this thesis, production, structural health monitoring and validation techniques for advanced fiber reinforced composites are investigated.

The fiber reinforced composites are well researched and widely used engineering material type. Generally the fibrous content carries the load while the matrix protects fibers from environmental effects and at the same time transfers load between fibers. As shown in figure 1.2, the high strength to weight ratio makes them widely used material

type in most notably aerospace, wind and marine industries. Compared to isotropic materials, fiber reinforced materials have more design flexibility which in turn increase their ability to match specific design requirements. Hybrid composites are such complex case where material behavior changes radically depending on the material configuration. For example, in 1972, the Avenger 21 power boat broke a world record thanks to 30% lighter, hybrid ribbon made shell [1, 2]. The majority of continuous fiber reinforced hybrid composites are either made of interply or intraply configurations. Interply hybrid composites are made of alternating single fiber laminas whereas variety intraply hybrid composites are consists of multiple fiber laminas.

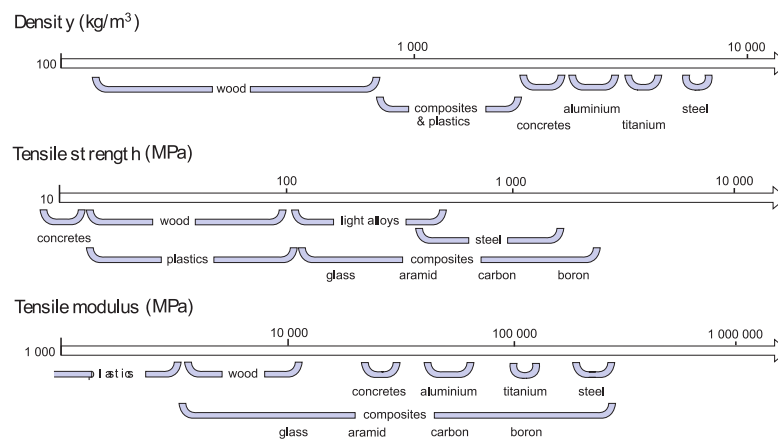


**Figure 1.2: Strength of several type of engineering materials[3]**

Structural health monitoring techniques are increasingly used to identify and track material behavior under operational circumstances. Fiber Bragg Grating (FBG) is an advanced sensing technique suitable for structural health monitoring especially when embedded into fiber reinforced composites. FBG sensor is sensitive to both strain and temperature. Thus FBG sensor can be applied to almost every case that a strain gage can be used. Due to nature of optical fibers, FBGs are immune to electromagnetic interference, corrosion and they can be spliced into multiple sensor arrays. The majority of applications utilize lightweight, noise free or ability to sense from long distances properties. Its relatively nonintrusive nature makes them suitable candidate for structural analysis of Fiber Reinforced Plastic (FRP). Figure 1.3 shows one application example of FBG sensors. In this study, a structural health monitoring system is developed in order to identify operational loads on the composite structure of the tilting train carbody[4].

This thesis in essence, will focus on structural health monitoring of unidirectional carbon/glass fiber interply hybrid composites by FBG sensors. Even though interply hybrid composites are widely used and easily produced, there exists a lack of in-depth research covering interply hybrids since beginning of 1990s. On the other hand, research on FBG sensors intensified since beginning of 1990s. Moreover there exists a limited amount of research studying strain transfer behavior of fiber reinforced composites by embedded FBG sensors. As a result, monitoring interply hybrids by FBG sensors makes a challenging, yet interesting thesis subject.

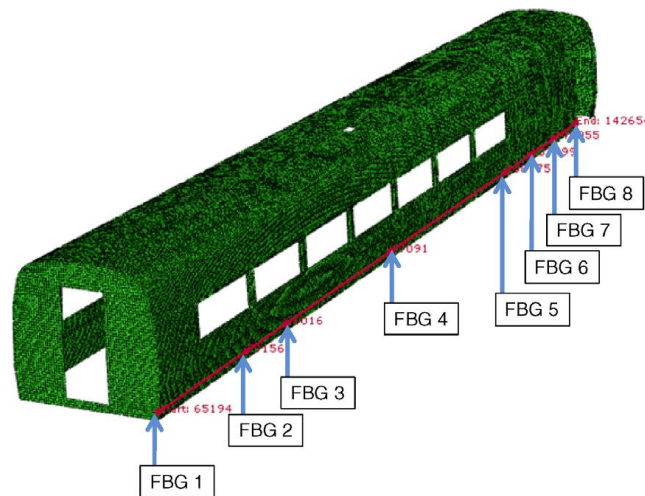


**Figure 1.3: FBG sensor locations on a train carbody [4]**

This thesis can be separated into 2 sections. The first part begins with design of manufacturing methods that can be used for smart specimen production. Since embedding sensors inside the composite is a significant challenge, manufacturing process design plays a crucial role in structural health monitoring. The second part is the experimental analysis of interply hybrid composite by using fiber Bragg gratings. In this part very large deformations are recorded by using silica based embedded FBG sensors for the first time. Moreover, by coupling multiple FBG sensors, the variation in ply behavior of the specimen is observed.

## 1.2. Outline of the Thesis

In this thesis, chapter 2 covers literature review on interply hybrid composites behavior, fiber Bragg grating sensors and flat composite specimen manufacturing

techniques. Chapter 3 covers manufacturing a new resin transfer molding unit. The chapter includes discussion of problems related to previous mold designs and engineering calculations. Chapter 4 covers experimental results and discussion of tensile testing of FBG sensor embedded carbon glass unidirectional interply hybrid composites. Chapter 5 concludes this thesis.

## CHAPTER 2

### Literature Review

#### 2.1. Hybrid Fiber Reinforced Composite

Hybrid composite is a result of reinforcement of two or more fiber types within a matrix. There are two major hybrid types, interply and intraply. Interply hybrid is achieved by stacking of two or more types single fiber laminas while intraply hybrid occurs when multiple fiber types are incorporated into a lamina either by woven single fiber tows or multiple fiber tows. Amongst others, Carbon/Glass interply hybridization is one of the popular hybrid composites. Carbon Fibers (CF) have high ultimate strength and stiffness while, Glass Fibers (GF) are relatively inexpensive and have high tensile strain. Therefore hybridization of carbon and glass laminas offers additional parameters to optimal design. One of the earliest reports of carbon/glass hybrid use in industrial application was for original Ford GT40 racing car body. The glass fiber composite structure was reduced 27 kg of weight from 42 kg by adding 1.4 kg of carbon fiber reinforcement. The resultant body had higher stiffness to preserve its shape at high aerodynamic forces and increased fatigue life [5].

Interply glass/carbon fiber hybrid composites show variety of response under tensile loading. Mathematical model of glass/carbon UD interply hybrid fiber reinforced composite can be developed by a modified Rule of Mixture (ROM) formula. Assuming perfect bonding between matrix and fibers, the strain equation is the following.

$$\epsilon_1 = \frac{\Delta L}{L} \quad (2-1)$$

Since the cross section of fibers and matrix equals to total cross section of specimen

$$A = A_f + A_m \quad (2-2)$$

One can find amount of stress distributed to fibers and matrix

$$\begin{aligned}\sigma_f &= E_f \epsilon_f \\ \sigma_m &= E_m \epsilon_m\end{aligned}\quad (2-3)$$

The total tensile stress equals to

$$P = \sigma_1 A = \sigma_f A_f + \sigma_m A_m \quad (2-4)$$

Since third dimension of the specimen is the same for every layer we can assume  $V_f = A_f/A$  and  $V_m = A_m/A$  resulting in

$$\sigma_1 = \epsilon_1 (E_f V_f + E_m V_m) \quad (2-5)$$

By using ROM principles one can obtain stress distribution between fiber types

$$\sigma_f = \epsilon_1 (E_c V_c + E_g V_g) \quad (2-6)$$

This leads to

$$\sigma_1 = \epsilon_1 (E_c V_c + E_g V_g + E_m V_{1-(v_c+v_g)}) \quad (2-7)$$

The behavior of interply GF/CF hybrid composite can be modeled as figure 2.1.

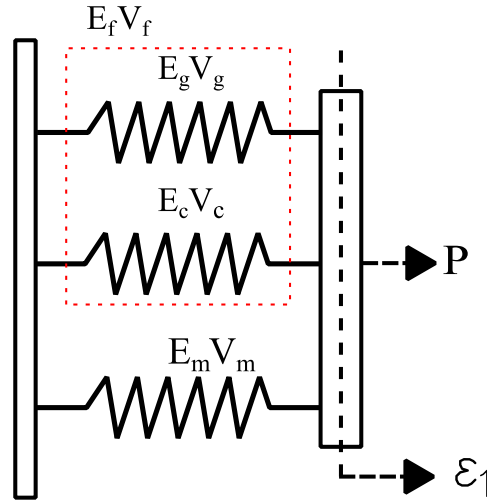


**Figure 2.1: Schematic model of unidirectional carbon/glass fibers interply hybrid composite**

From the figure, one may notice that fibers and the matrix behave as parallel springs. As a result of parallel spring type structure, the composite may carry the load when one of the fiber types fails. Depending on GF to CF volume fraction ratio, either

progressive or sudden failure occurs. As a result of higher modulus and lower ultimate strain properties of CF, initial failure occurs at CF reinforcements. At this point, if GF reinforcements do not have enough load bearing capacity to transfer the additional load, the GF reinforcements break and the failure occurs suddenly. However if there is some capacity left in GF then the GF reinforcement can transfer additional loads resulting in progressive failure.

When progressive failure occurs, distinct slopes and sharp load drops can be seen at stress strain plot. In figure 2.2, dashed line “a” denotes the carbon fiber reinforced composite (CFRC) while “d” denotes glass fiber reinforced composite (GFRC), solid line “b” denotes carbon fiber rich hybrid composite whereas solid line “c” denotes glass rich hybrid composite.

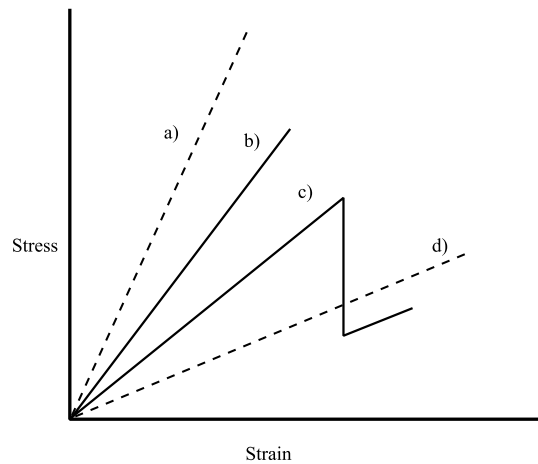


**Figure 2.2: Stress versus strain behavior with respect to CF to GF ratio**

One may notice that CF and GF composites have best ultimate strength and ultimate strain respectively. Moreover as mentioned earlier, GF to CF ratio significantly affects failure mode of the material.

A phenomenon called hybrid effect is noticed in hybrid materials when first major failure of hybrid material occurs at higher strain rates than CF. The hybrid effect is first reported by Hayashi in 1972 [6]. The work indicates that failure of low elongation fibers tend to occur at higher strain rate when hybridized with high elongation fibers. This phenomenon first attributes to compressive thermal strains occurred due to difference in thermal expansion coefficients between glass and carbon fibers. However later it is observed that thermal strains account less than 10% of hybrid effect[7]. Moreover due

to different shrinkage rates, hybrid composite has to be symmetric with respect to its neutral axis, otherwise thermal strains can lead to bending-stretching coupling.

## 2.2. Fiber Bragg Gratings

### 2.2.1. Optical Fibers

Optical fibers are most commonly based on three layers, shown in figure 2.3, which are referred to as, core, clad and coating. Light entering into the fiber propagates by total reflection due to refractive index difference between clad and core. To trap the light inside the core, the refractive index of the clad has to be lower than the core's. The coating layer provides variety of mechanical strength to the fiber depending on the coating material type. Most telecom fibers offer acrylic coating which is easy to handle and strip. On the other hand polyamide coating provides better mechanical strength and chemical resistance. Acrylic coating is roughly 100  $\mu\text{m}$  thick whereas polyamide coating is 15-20  $\mu\text{m}$ .

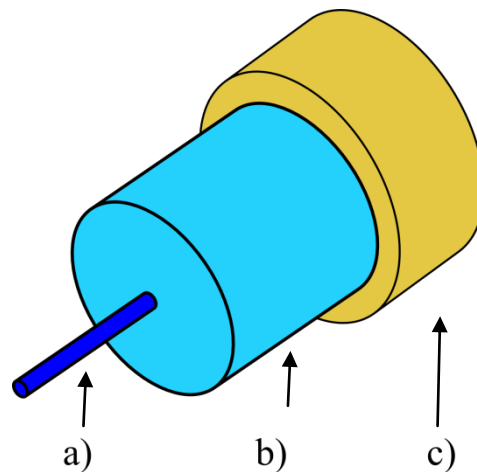


**Figure 2.3: Optical fiber layers, a) the core, b) the cladding and c) protective layer**

### 2.2.2. Fiber Bragg Gratings

Fiber Bragg grating is an optical wavelength filter that reflects Bragg wavelength and transmits rest. In fiber Bragg gratings were first demonstrated by Ken Hill in

1978[8]. This method which is referred as Hill Gratings uses visible light propagating inside the fiber. In 1989 Gerald Meltz et al. discovered FBG writing by interference pattern of ultraviolet laser light[9]. In this method a UV beam is separated and interfered to create periodic intensity distribution along the interference pattern. When the resultant beam applied to the side of the germanium doped optical fiber, periodic refractive index variations occur due to germanium being photosensitive to UV light.

FBG sensor in structural monitoring is a well researched and established topic. The Bragg wavelength which is shown by eq. ( 2-8). is determined by Bragg condition.

$$\lambda_B = 2n_{eff}\Lambda \quad (2-8)$$

Here  $\lambda_B$  is the Bragg wavelength,  $n_{eff}$  is the effective refractive index of FBG, and  $\Lambda$  is the grating period. The change of  $\lambda_B$ , eq. ( 2-9), is determined by temperature and strain components of FBG.

$$\frac{\Delta\lambda_B}{\lambda_B} = (\alpha + \xi)\Delta T + (1 - \rho_e)\varepsilon \quad (2-9)$$

Here  $\alpha$  is the thermal expansion coefficient of fiber core,  $\xi$  is the thermo-optic coefficient of fiber core,  $\Delta T$  is the temperature change at FBG region,  $\rho_e$  is the effective photo-elastic constant of fiber core, and  $\varepsilon$  is the axial strain of FBG part. If there is no temperature change close to the FBG region then the eq. ( 2-10) can be reduced to:

$$\frac{\Delta\lambda_B}{\lambda_B} = (1 - \rho_e)\varepsilon \quad (2-10)$$

As shown in the figure 2.4 essentially FBG behaves as a reflective band filter that is sensitive to strain and temperature.

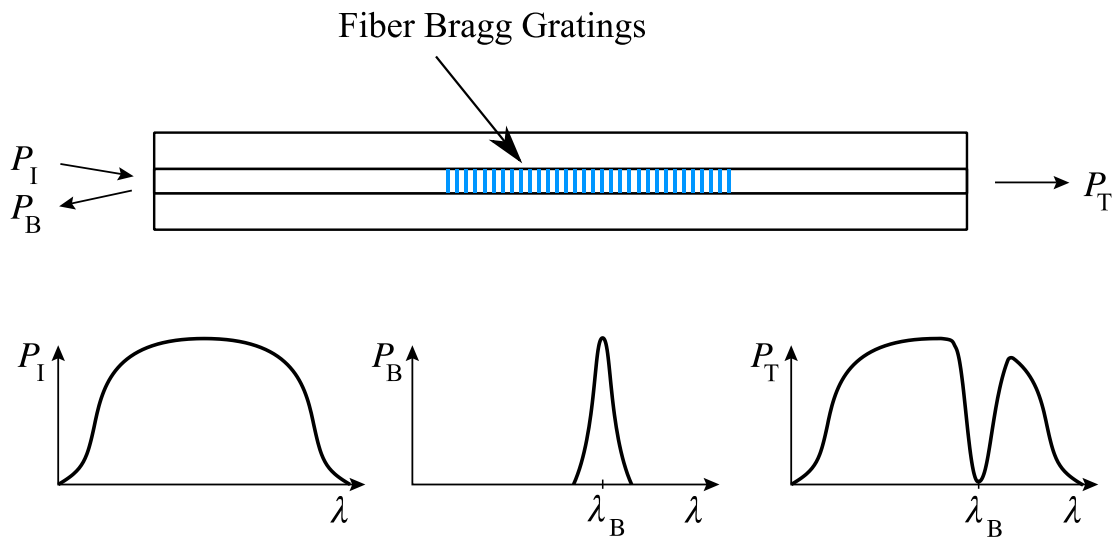


**Figure 2.4: Fiber Bragg gratings**

Due to FBG's low density non-intrusive nature, there have been numerous research performed on behavior of FBG embedded into fiber reinforced polymer matrix composites. Tao et al. [10] states that for FBG sensor accurately measuring strain in fiber reinforced composites: optical fiber in host media should be minimal intrusive, measured axial strain  $e_1$  on optical fiber should represent actual strain of surrounding bulk material, Poisson's ratio should be constant during measurement. Kuang et al. [11] carried out FBG spectra behavior experiments on variety of reinforcement materials and found out that two identical specimen can lead to different FBG spectra behavior due to FBG or fiber movement during manufacturing or resin flow. Moreover in the same work, the author states that transverse fibers touching the FBG may provide non-uniform residual stress which in turn results in peak splitting. In a parallel work, Lu et al. [12] experimented on embedding FBG transversely and longitudinally in unidirectional carbon fiber reinforced plastics. The results showed that longitudinal placement of FBG has almost no effect on reflected spectrum whereas transversal placement resulted in two distinct peaks. Therefore it is important for proper measurement to have optical fiber nested between longitudinal reinforcement fibers. Furthermore, optical fiber itself is sensitive to a phenomenon called microbending [13]. The light passes through single mode optical fiber by internal reflections. The angle of reflection is a function of refractive index ratio of core and cladding material. When position of internal reflective surface moved, then a portion of light approach to the reflective surface at a degree outside of reflection angle limits. Instead of being

reflected, as shown in the figure 2.5 this portion of the light is refracted and lost away from the core. Therefore microbending between interrogation system and FBG severely decreases the intensity of the reflected light.

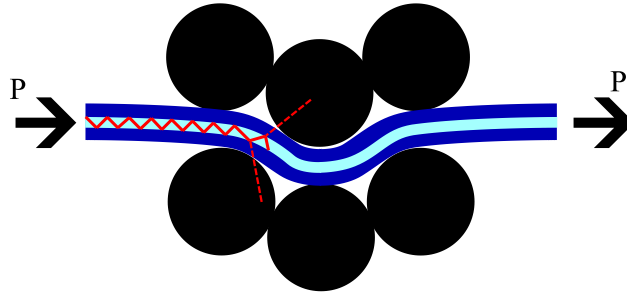


**Figure 2.5: Microbending in optical fibers**

Kang et al. [14] experimented on effects of strain gradient on various length of FBG. In his work, utilizing a cantilever beam setup, concluded that at especially large deformations between 10, 5 and 2mm FBG gratings, 2 mm grating is the most insensitive to strain gradient along the optical fiber while 10 mm grating has the most susceptibility. Moreover, similar to previous result, reflectivity of 2 mm grating almost was not affected by large deformation whereas reflectivity of 10 mm grating decreased by 81% at same deformation. The work concluded a strain gradient limit with respect to grating length as shown in the figure 2.6.

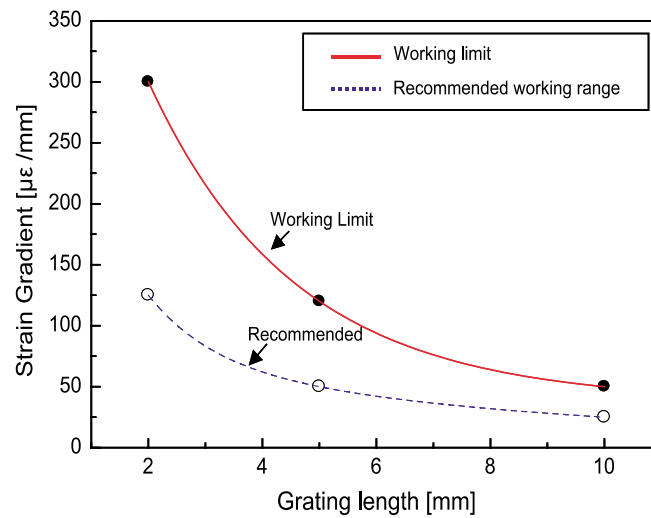


**Figure 2.6: FBG strain gradient sensitivity of strain gradient with respect to grating length [14]**

Another well documented area is the mechanical limits of fiber Bragg gratings. Due to diversity of application field there have been numerous research performed on mechanical effects of FBG writing process on optical fiber. For most of FBG writing process an optical fiber is stripped from its coating by either chemical or mechanical method and then subjected to UV beam pulses. Usually chemical stripping of coating refers to immersion of optical fiber in a hot sulfuric acid bath whereas mechanical stripping is done by a series of blades. Most of the researches done on this area conclude that major mechanical strength degradation occurs due to stripping of optical fiber. Moreover UV beaming of optical fiber degrades mechanical strength further although not as significant as stripping of coating [15-17]. Skontorp [16], in his experiments found out that ultimate strength and strain of 145µm diameter polyimide coated fiber generally are 4.8 GPa and 5.5%. However in a stark contrast, hot acid stripped and then recoated optical fibers performed much lower at 0.7 GPa and 0.9% respectively.

### 2.3. Fiber Reinforced Composite Manufacturing Methods

Manufacturing of fiber reinforced composite plates can be achieved by variety of techniques. The major manufacturing processes are hand lay-up, bag molding, vacuum infusion, resin transfer molding and autoclave. There are other widely used fiber

reinforced composite manufacturing methods, however, they are either not useful for flat rectangular specimen manufacturing (filament winding) or not suitable for sensor embedding (pultrusion). Therefore these manufacturing processes will not be covered in this thesis. A comparison of performance versus production volume is given in the figure 2.7 [3]. This figure shows that prepregs and advanced RTM solutions produce near identical results.

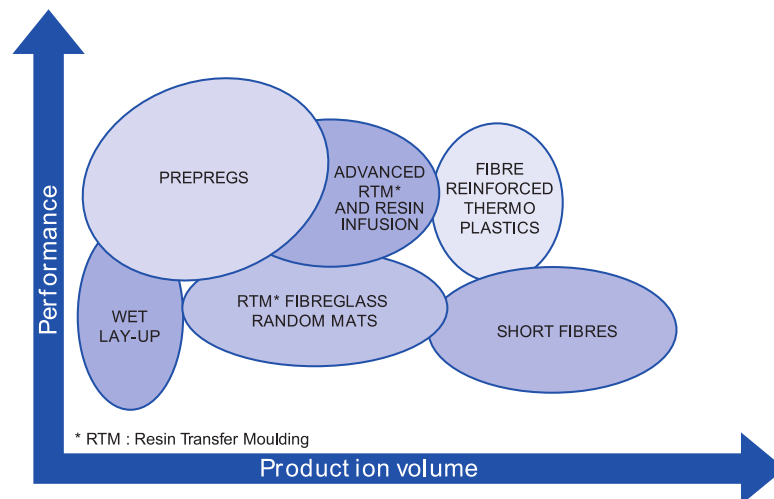


**Figure 2.7: Production and performance characteristics of several type of manufacturing methods [3]**

### 2.3.1. Hand Lay-up

Hand lay-up which is also called as wet lay-up manufacturing technique, is a simple and widely implemented composite production form. The manufacturing operator manually positions dry reinforcement plies on the mold with subsequent resin application. Then the applied resin is distributed evenly across the reinforcement with a soft roller. Following the resin distribution a metal roller applied to reinforcement surface to remove void content. The process is repeated until desired thickness and ply number achieved. For further increase in volume fraction, vacuum bagging can be applied to wetted part. Due to necessary manual labor, the quality of output product is greatly related to operators' skill. A representative schematic is given in the figure 2.8.

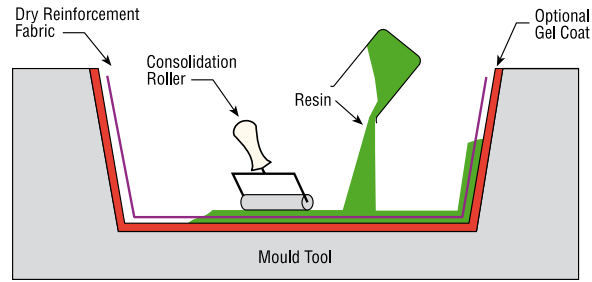


**Figure 2.8: Hand lay-up schematics [18]**

Due to the nature of hand lay-up, FBG embedding can be a arduous process for two major reasons. First, FBG has to be positioned while some of the plies are already wetted. As the optical fiber is in touch with wet and sticky surface, positioning of FBG is relatively difficult. In addition to this, rolling the resin after embedding FBG into ply may force FBG to dislocate its desired position. Last but not least, since resin and hardener are already mixed and activated, the allocated time for FBG positioning is relatively short.

### 2.3.2. Bag Molding

Bag molding or vacuum bagging is a more advanced composite manufacturing method based on hand lay-up technique. In addition to steps of hand lay-up technique, bag molding utilizes a flexible bag material and vacuum pump in order to produce higher quality components. The process begins with hand lay-up procedure. After the component is fully wet, peel ply, breather, necessary hosing and flexible bagging material are applied to the component in order. The schematics of component layers can be seen in figure 2.9.

The peel ply is a layer which provides non-sticking effect between breather fabric and resin. The function of breathers is to distribute atmospheric pressure around the component and a reservoir for excessive resin content. In order to maintain vacuum over the entire production process, the flexible bagging material together with molding unit encapsulates the component.

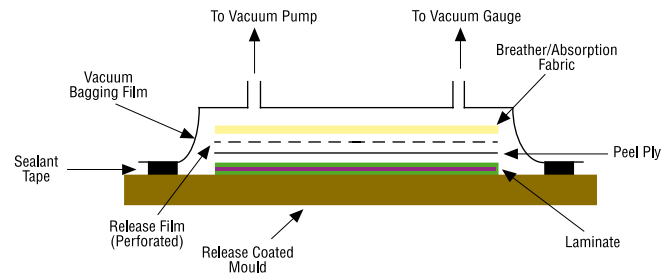


**Figure 2.9: Vacuum bagging [18]**

Utilizing bag molding method for placement of FBG sensor includes all of the hassle of hand lay-up technique and also additional care for ingress locations. Vacuum sealing of optical fiber at ingress location requires additional equipment to guide optical fiber through sealant putty. Otherwise removal of putty at the end of the manufacturing process may break optical fiber.

### 2.3.3. Vacuum Infusion

The vacuum infusion process uses several steps in order to complete the part. The process begins with placement of all dry reinforcement on the mold. Then bagging material and sealing putty is used to cover upper surface of the mold. Adequate numbers of inlet and outlet ports are placed through the bag. An optional spiral hose inside the bag can be used to distribute resin more effectively. After the bag is fully vacuumed and leak proof, the resin is let through the inlet ports. Depending on the type of resin hardener mix, curing process can occur at room temperature or above. The process can be summarized in figure 2.10.

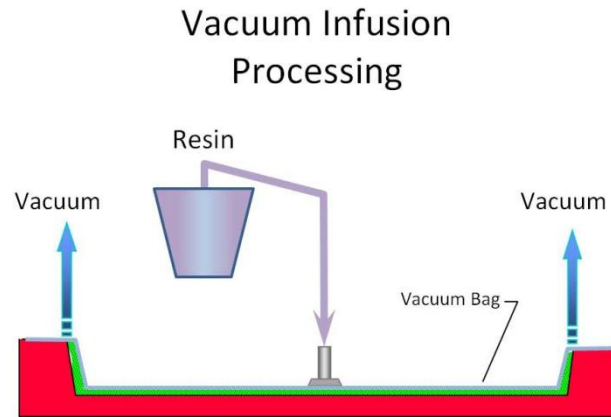


**Figure 2.10: Vacuum infusion [19]**

Vacuum infusion provides one of the easiest methods for FBG placement. Since vacuum infusion is mostly a dry process, the FBG placement can be done prior to composite production with virtually unlimited allocated time. Moreover absence of any rolling effect and mostly mistake proof nature of VI increases the positional accuracy of the FBG embedding.

#### **2.3.4. Resin Transfer Molding**

Resin Transfer Molding (RTM) technique requires two separate mold unit to manufacture a part. A comparison between figure 2.10 and figure 2.11 may reveal similarities with vacuum infusion process. The process begins with placing the dry reinforcement material on lower mold surface. Upon clamping upper and lower mold, resin can be infused through inlet channels. During the infusion process, pressurized resin displaces trapped air inside the dry reinforcement to the outlet ports. The mold can be manufactured from variety of engineering materials depending on output requirements. For low unit number of production, generally molds made of composite are used whereas for high unit numbers high stiffness metals are obvious choice.

## Resin Transfer Molding

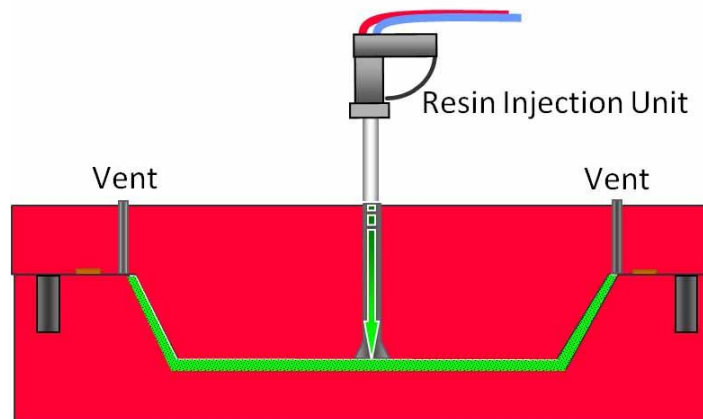


**Figure 2.11: Resin transfer molding, in some applications vents are vacuumed [19]**

As a result of highly repeatable production nature of resin transfer molding unit, embedding of FBG sensors lead to repeatable experiments. However since RTM is based on pressurized rigid molds, optical fiber ingress points cause great design challenges. In addition, sensor embedding flexibility of RTM method is one of the least compared to other production methods.

### 2.3.5. Prepreg

The prepreg is commercial form of fiber reinforcements where resin is pre-impregnated and partially cured [20]. Correspondingly, almost all of the prepreg materials have elevated curing temperatures to enhance shelf life. Most of prepreg materials are available in roll form in which the operator manually cuts and places the plies until a desired level of part thickness is achieved. After that the stacked plies are cured above room temperature by autoclave or vacuum bagging technique. Otherwise excess resin and void content within the final part may reduce the mechanical performance.

### 2.3.6. Autoclave

Autoclave is a high pressure and high temperature cylindrical vessel used for high quality and complex composite manufacturing. The process can be defined as an extension for prepreg or vacuum bagging manufacturing method. The part should be first wetted outside and vacuumed. After this step, the component can be placed inside the chamber and cured at necessary conditions. Essentially, an autoclave, in figure 2.12, behaves as a high pressure atmosphere on composite part.

The autoclave vessel is a relatively expensive production tool, targeting mostly wind, automotive and aerospace industries especially in areas where the quality and repeatability are crucial. High pressure exerted on wet fabric displaces excessive resin content and trapped voids to vacuum port. The pressure coupled with high temperature lowers the resin viscosity so that the resin can penetrate into denser fibers. Sensor embedding process requires no additional care apart from degrading effect of high temperature on optical fiber and FBG.

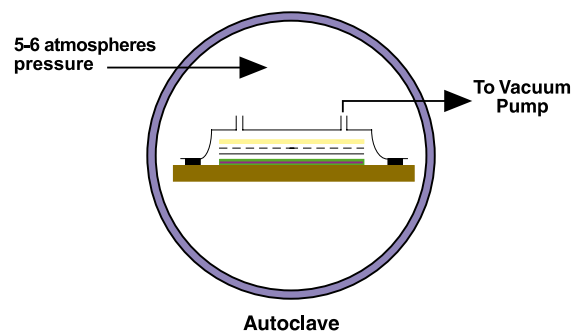


**Figure 2.12: Autoclave vessel [18]**

## **CHAPTER 3**

### **Fiber Reinforced Composite Manufacturing Method Design**

In this chapter, design and manufacturing steps of resin transfer molding and vacuum infusion will be shown in depth. As discussed in previous chapter, RTM and vacuum infusion methods have advantages and disadvantages. It is safe to say that the repeatability of RTM method enables in-depth experimental mechanics analysis possible whereas sensor embedding versatility of the vacuum infusion method makes it a good candidate for the embedded sensor behavior analysis. Since structural health monitoring of composites focuses on mechanics and sensor behavior, manufacturing method design for embedding techniques is an important step.

Following is the structure of this chapter. In the first section, the design and shortcomings of preceding RTM unit in Advanced Composites and Polymer Processing Laboratories (AC2PL) will be discussed in detail. After that, the revision that addresses some of the shortcomings of the preceding design will be covered. In the third section, the design of a novel RTM unit will be analyzed. In the last section, a manufactured vacuum infusion unit will be reviewed.

#### **3.1. Resin Transfer Mold Design**

##### **3.1.1. Preceding Design**

The preceding design required intensive modifications after serving 4 years of continual service. The mold first designed in such a way that variety of experiments can be feasible. Different kind of molding surfaces could be attached to the molding unit in

order to produce different specimen geometries. Moreover sensor attachment ports can be utilized as either pressure sensors or FBG ingress locations. The mold itself, visible in figure 3.1, used several different kinds of materials in different locations in order to perform optimally. The load carrying structure was made of galvanized tube steel or welded steel panels. An aluminum block together with thermal water carrying copper pipes acted as heat distributor. The glass window bonded to upper lid provided visual monitoring of production process. The mold surface was made of aluminum for machinability. Two high temperature resistant silicone o-rings were used for vacuum and sealing purposes.

The mold operation can be summarized in order as below:

- The mold is prepared by a set of sealer and release agents
- The fabric is placed adequately
- If required FBG sensors are embedded as well
- The upper lid is closed and clamped
- The mold is heated to the elevated temperatures and vacuumed
- The resin mixture is injected to the mold when ready
- The speed of the flow and amount of bubbles trapped inside are measured from monitoring window
- When the injection process is finished, the inlet and outlets are sealed and mold is heated to curing temperature
- The composite is then cured at manufacturers advised temperature and duration
- Finally the mold is unclamped and the composite is removed



**Figure 3.1: Preceding RTM; rectangular glass is visible**

After continual operation there were few issues needed to be addressed with modifications in order to increase production efficiency of the mold. The main problem originated from monitoring window being smaller than mold surface area. The inlet and outlet ports were initially situated at upper lid. Therefore the monitoring window was designed to be smaller than operating area. To fix window glass in its place in aluminum lid high temperature high strength Momentive RTV 159 silicone adhesive was used. Although the adhesive itself is chemically inactive to epoxy resin, it is susceptible to mold preparation agents. Repeated use of mold degraded adhesive strength that the adhesive had to be renewed annually. When the surface agents were avoided in adhesion regions, the epoxy resin tended to bond to those regions. This led to high loads on glass window when the lid was opening. Moreover, the absence of rigid single surface at the top section resulted in fluctuations of measured thickness at the composite plate.

### 3.1.2. Design Revision

The basis of the mold design revision is extending the window glass over o-ring seals. The figure 3.2 shows extended glass size. One may notice that shape of viewing glass is exactly the same as o-ring canals. This revision leads to multiple benefits. First, thickness variation of composite plate is greatly reduced due to uniform upper surface.

Second, the absence of epoxy resin close to adhesion region enabled stronger adhesive to be used in those regions. Last but not least, life time of the glass itself is greatly extended.

In order to extend the size of glass the inlet and outlet ports are moved to lower lid.



**Figure 3.2: Revised RTM; shape of the glass is similar to o-ring path**

### 3.1.3. The New Design

Although the revision extended lifetime of RTM unit, there still exists problems that affect quality of the output. The first problem is a phenomenon known as “Race Tracking”. Race Tracking occurs when reinforcement fabric is not properly cut and cannot fill the mold adequately which results in the resin free flowing through void canals instead of wetting the fabric. Another problem is adhesion of glass to aluminum. The problem arises due to two different reasons. The first one is that there are not many commercially available adhesive that can be used with tempered glass and aluminum at the same time while continuous operating temperature is above 80 degrees Celsius. The other one is the difficulty of changing the glass as glass breaks occasionally leaving

adhesive on aluminum surface. Moreover and due to manufacturing errors and tolerance stacking, plate thickness varies greatly on single plate depending on the location of the measurement. As a result, a new RTM model, shown in figure 3.3, is developed to answer the problems above.

The new mold functions in a similar way as the preceding mold. There are two molding surfaces which are held together by a series of mechanical clamps. Similar to the preceding mold, the upper part is glass whereas lower part is made of aluminum. Instead of using adhesives an additional aluminum frame is used to hold glass in its position securely. Therefore in case of glass failure a fast change can be easily made.



**Figure 3.3: Render image of the new RTM**

Load bearing structures are made of either 50 mm square profile or 10 mm thick plates both made of steel. There are two 15 mm thick aluminum plates for pipe guiding and heat distribution purposes. Ports for sensor input and resin inlet outlets are all situated in aluminum part of the mold. There are 4 important features on the lower surface. From the figure 3.4, shown as number 1, there are two o-ring spaces surrounding the mold area. Normally the inner one seals the mold but in case of leakage the outer one stops resin from spreading to unwanted places. Second mark shows sensor positions on the mold surface. These holes can be used not just for FBG but for other type of sensors such as pressure when used with adequate fittings. These sensor

locations are designed such that variety of FBG distribution configurations can be applied for a given plate.

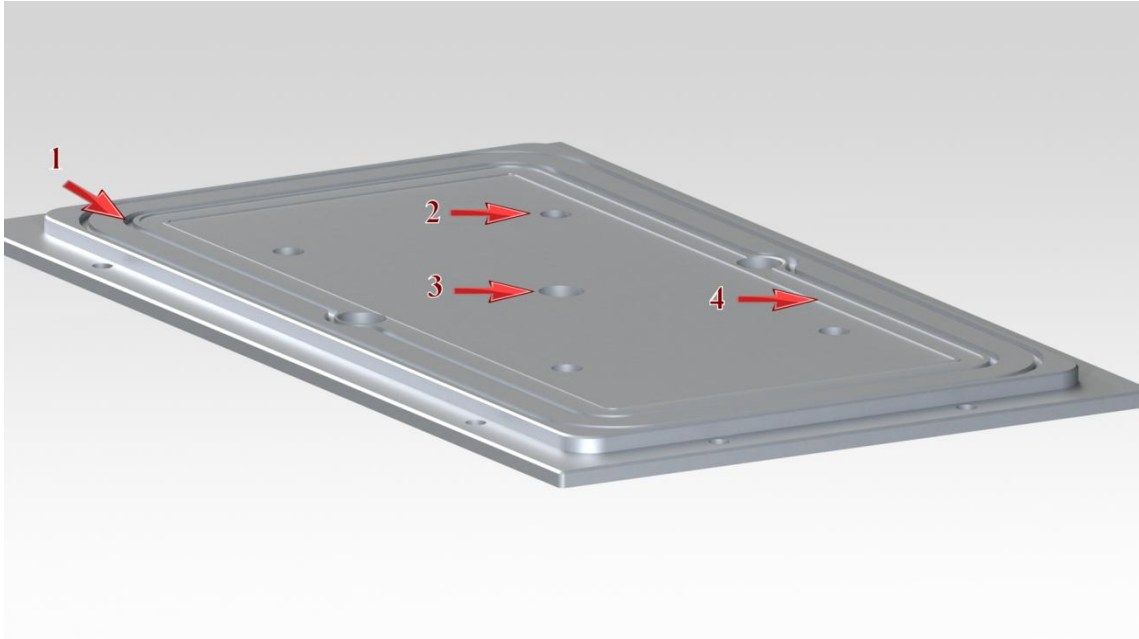


**Figure 3.4: Important molding surface features**

Resin inlet and outlet ports are designed to be versatile such that any of the three ports can be configured as inlet or outlet. In addition there are flow channels surrounding the mold area for better resin distribution. Depending on the experiment, the user can adjust the port according to desired resin flow path. figure 3.5 shows one of the possible flow configurations. Thus resin can be distributed more evenly across the mold surface. As described previously race tracking can often leave unwetted spots in the middle of the mold area. Therefore a more evenly distributed resin is better for healthy experiments.

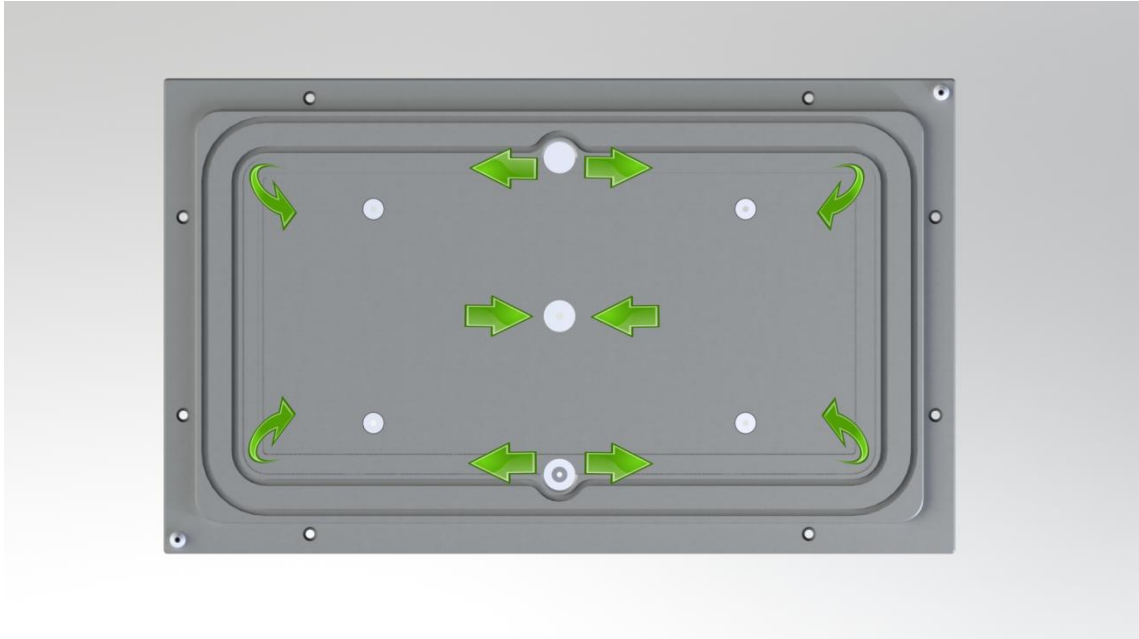


**Figure 3.5: A flow path example**

Due to excessive use of metals throughout the mold the cover part is calculated to be 84 kg. Thus, there are two inverted gas springs (pulling type) connected to cover and bottom of the mold for health and safety reasons. The figure 3.6 shows load vectors acting on the RTM unit. Blue and orange arrows show the position of center of rotation. All of momentum curves shown in the figure 3.7 are calculated with respect to this center.

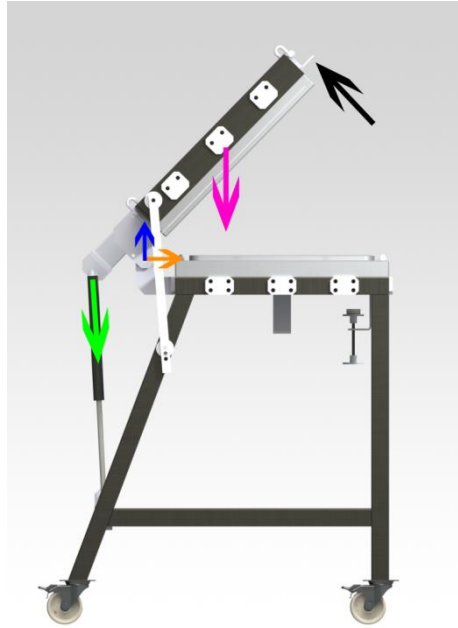


**Figure 3.6: Load vectors**

Figure 3.7a, represents the proportional moment for the force vector of the gas springs and the center of gravity and gravitational force vector as a function of angle with respect to the horizontal positioning of the mold cover. Figure 3.7b shows the required force of which the operator should apply to lift the cover as a function of cover angle.

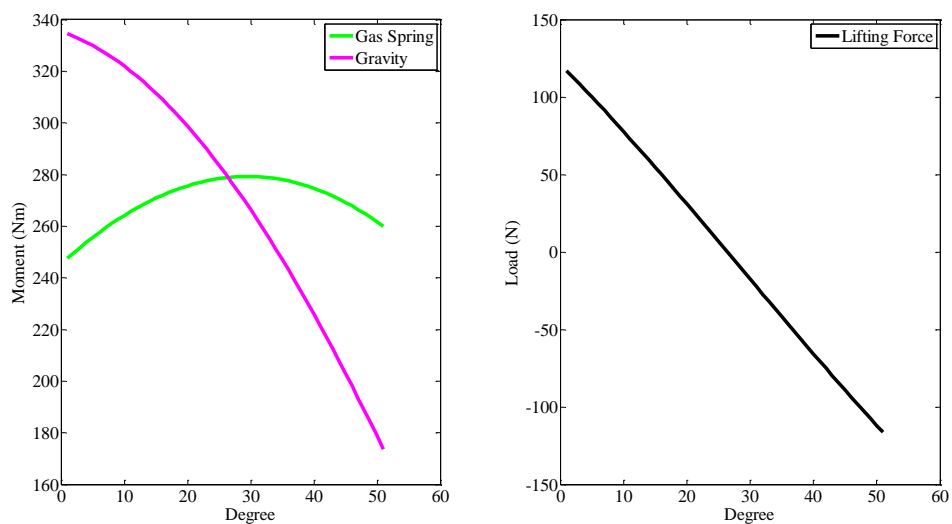


**Figure 3.7: a) Moment as a function of cover angle, b) Lifting force required by operator at the particular angle**

The gas springs are designed in such way that they do not change the state of the cover of the mold until the operator overcomes the remaining force. As a result, the operator would need only approximately 100 N of force to lift the cover.

Finite element models are developed in COMSOL Multiphysics environment in order to simulate operational loads on critical components. There are two critical components identified in molding unit. The first one is the pulling arm of the upper lid and the second one is the hinge. There exists a symmetric boundary at pulling arm model. Therefore the model is cut into half and a symmetric boundary condition defined on newly created surface. The models evolved after many simulation runs and final results are shown below in the figure 3.8 and figure 3.9. Since St-52 steel has yield tensile strength of 350 MPa, strength of the components are sufficient [21].

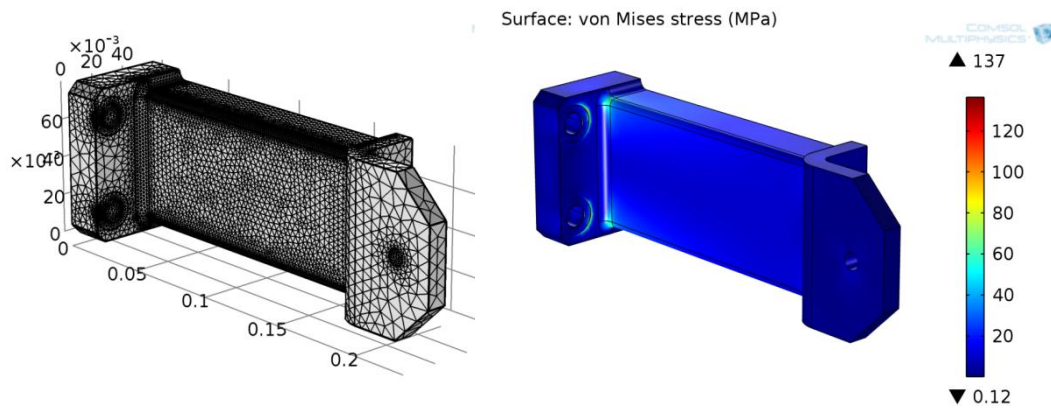


**Figure 3.8:** a) Mesh model of mold cover – gas spring connecting arm, b) Stress result

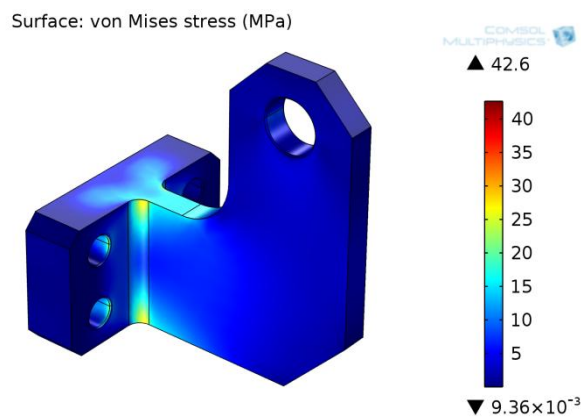


**Figure 3.9:** Loading results at cover hinges

### 3.2. Vacuum Infusion Unit

As explained in prior sections, vacuum infusion method is the most flexible production method for FBG sensor embedding. Therefore a new unit is designed and manufactured for structural health monitoring purposes. The unit is made of three sections. The first part is network of copper pipes for heating and cooling. The second part is aluminum block for heat distribution and solid base. The last part is the curing surface made of tempered glass. Since the size of the glass is 75 x 65 cm, either large or multiple type of plate configurations can be produced. The unit is designed in such way that it can be utilized by variety of composite production method. Considering the flat surface as the only rigid boundary, there are many opportunities to ingress optical fiber inside the composite. Therefore enhanced monitoring techniques become possible. As a result, a vacuum infusion next to RTM increased our laboratory production efficiency and output. The figure 3.10 shows variety of possible applications.

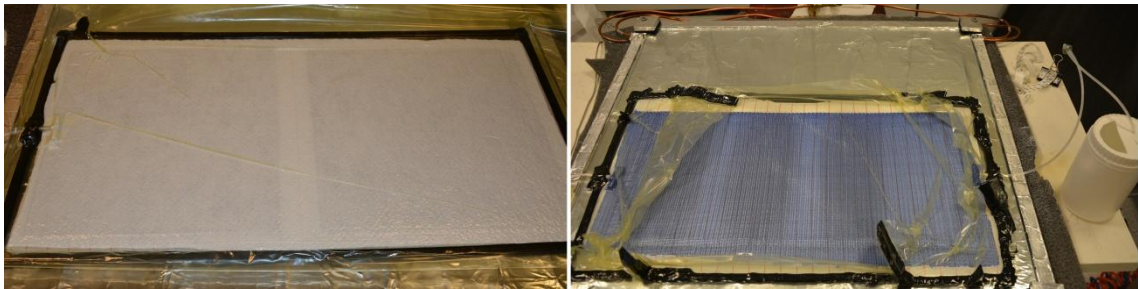


**Figure 3.10: a) prepreg manufacturing by vacuum infusion table, b) nanophase reinforced composite manufacturing**

## CHAPTER 4

### Experimental Composite Specimen Testing

#### 4.1. Mechanical Analysis of Advanced Composites

In this subchapter works performed experimentally within SANTEZ project titled “Development of Multiaxis Multilayer Fiber Reinforced Composites” will be described in detail. The project is developed cooperatively by Sabanci University and Yonca-Onuk JV. The aim of the project is to develop lighter and cheaper fiber reinforced composite solutions to be used in advanced marine vessels. The following figure summarizes the project schedule.

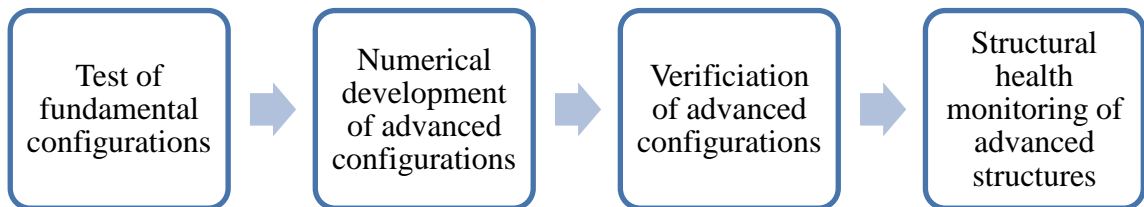


**Figure 4.1: Composite development stages**

The project can be separated into two distinct topics. The first part is theoretical and numerical development while the second part is experimental testing and verification. The theoretical part consists of derivation of necessary formulation representing advanced multiaxis multilayer composite behavior while the numerical part consists of numerical solutions to those formulations. The experimental part has two stages. The first stage is experimental measurement of mechanical properties of fundamental composite configurations. The findings of these basic composite will be ported to numerical program to be used for simulation of more advanced configurations. In next stage, experimental results of the advanced configurations will be used for

verification of numerical solutions. Furthermore, these newly developed advanced composites will have embedded sensors to monitor their behavior under operational loads. As a result, the vessel hull developers will have enhanced resources for development of lightweight structures.

A new composite testing laboratory is built in partnership with Instron Turkey to be utilized for the mechanical tests. A high frequency fatigue capable Universal Testing Machine (UTM), Instron 8801 shown in the figure 4.2, is supplied to the lab. The UTM has many fixtures and sensors tailored for specific ASTM standards.



**Figure 4.2: Mechanical testing laboratory setup**

The experimental work started by ASTM D3039 tension tests of fiber reinforced composite specimens. Most of the specimen production and preparation are done by Yonca-Onuk J.V. operators. According to the ASTM D3039 specimen geometry is rectangular shape, 250 mm long, 25 mm wide. The middle 150mm section is gauge length while upper and lower 50 mm part is for gripping. The height of the specimen is a user parameter and depending on the failure modes, specimens can be either tabbed or non-tabbed. General consensus states that a failure within grip section shows requirement for tabbing. In addition, more the orthotropic the material is, the greater necessity for tabbing. Since the testing machine had special grips that do not impair

matrix reinforcement integrity, initially there was no need for tabbing. However in later stages, testing was hampered by equipment malfunction which will be shown in the following part.

The testing procedure has two sections. The first section is used to calculate chord modulus of the specimen. Each specimen is tested up to 5000  $\mu\epsilon$  for 5 times. Repeated test cycle increases the statistical accuracy of the test results. Then the specimen is subjected to tensile loading until the failure. The figure 4.3 shows common test setup for tensile specimens.

Tensile testing results of one of the basic configuration,  $-45/+45^\circ$  biaxial carbon fiber reinforced composite, are shown in table 4.1 and table 4.2. The averaged data of chord module and ultimate strength form the basis of numerical code. The low standard deviation shows that manufacturing and testing of the specimen are repeatable.

**Table 4.1: Chord modulus results of the  $-45/+45^\circ$  CF specimen**

	Specimen Label	Thickness (mm)	Width (mm)	Maximum Tensile Stress (MPa)	Chord Module between 2500-5000 $\mu\text{sn}$ (MPa)
1	B1	7.17	25.13	32.85	5456
2	B2	7.17	25.13	33.76	5750
3	B3	7.17	25.13	33.93	5797
4	B4	7.17	25.13	33.90	5842
5	B5	7.17	25.13	34.16	5844
6	D1	6.97	25.04	30.70	5327
7	D2	6.97	25.04	32.16	5479
8	D3	6.97	25.04	32.33	5505
9	D4	6.97	25.04	32.30	5509
10	D5	6.97	25.04	32.48	5545
11	F1	6.91	25.08	30.83	5124
12	F2	6.91	25.08	31.52	5408
13	F3	6.91	25.08	31.75	5400
14	F4	6.91	25.08	31.78	5393
15	F5	6.91	25.08	31.56	5383
16	H1	7.07	24.98	31.59	5396
17	H2	7.07	24.98	33.00	5621
18	H3	7.07	24.98	33.09	5584
19	H4	7.07	24.98	32.81	5669
20	H5	7.07	24.98	33.15	5656
21	I1	7.08	25.02	32.45	5238
22	I2	7.08	25.02	33.07	5617
23	I3	7.08	25.02	33.32	5675
24	I4	7.08	25.02	32.71	5660
25	I5	7.07	25.02	33.38	5666
Max		7.17	25.13	34.16	5844
Min		6.91	24.98	30.70	5124
AVG.		7.04	25.05	32.58	5542
STD. DEV.		0.09249	0.05244	0.93996	184.01800

**Table 4.2: Ultimate tensile stress results of -45/+45° CF specimen**

	Specimen Label	Thickness (mm)	Width (mm)	Maximum Tensile Stress (MPa)	Tensile Stress at Break (MPa)
1	B	7.17	25.13	65.41	23.90
2	D	6.97	25.04	63.60	31.79
3	F	6.91	25.08	61.96	22.06
4	H	7.07	24.98	64.19	12.53
5	I	7.08	25.02	65.23	2.04
Maximum		7.17	25.13	65.41	31.79
Minimum		6.91	24.98	61.96	2.04
Average		7.04	25.05	64.08	18.47
Standard Deviation		0.10149	0.05745	1.40000	11.45585

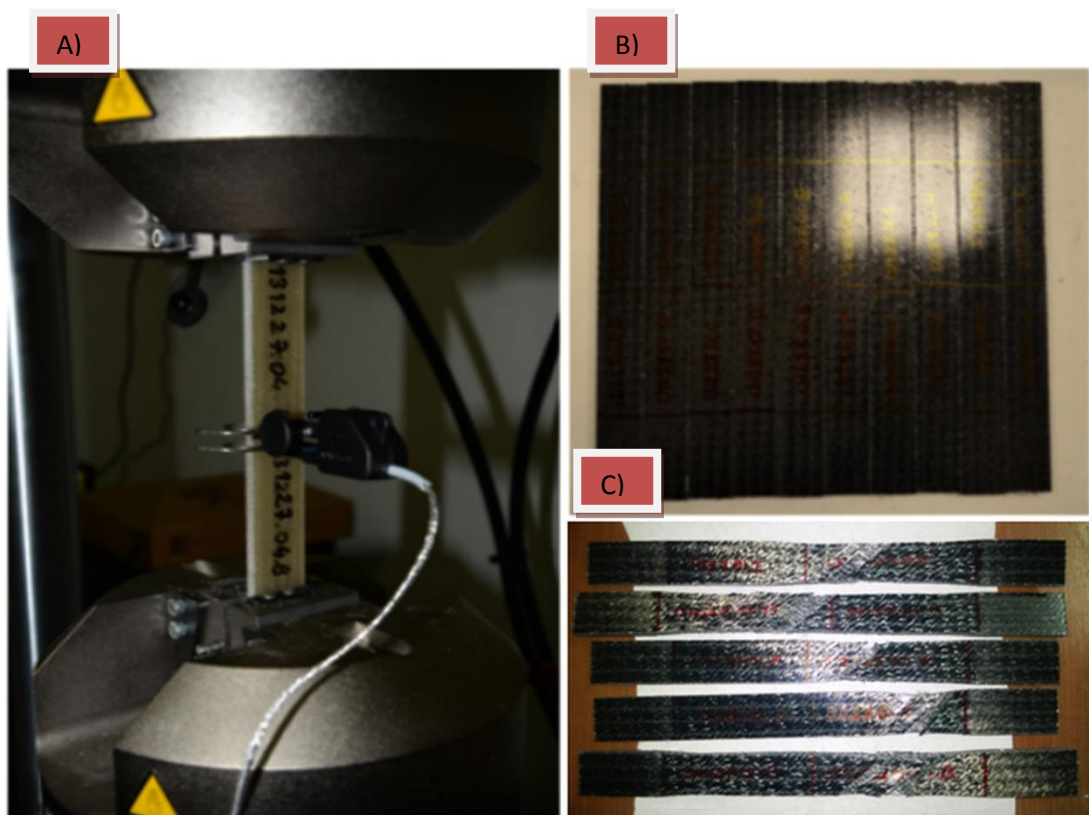


**Figure 4.3: a) An example chord modulus testing setup, b) specimens prior to the testing, c) specimens after the testing, notice the necking behavior**

As previously stated some of the equipments were malfunctioning and severely costing time and resources. One of the significant problems was the reliability of the transverse extensometer. The transverse extensometer is a very critical component for mechanical tests especially for measuring Poisson ratio of the specimen. To prove extensometer malfunction, a specimen with transverse strain gage was prepared. The

figure 4.4 shows results of variation in extensometer measurements even though the same specimen was tested twice.

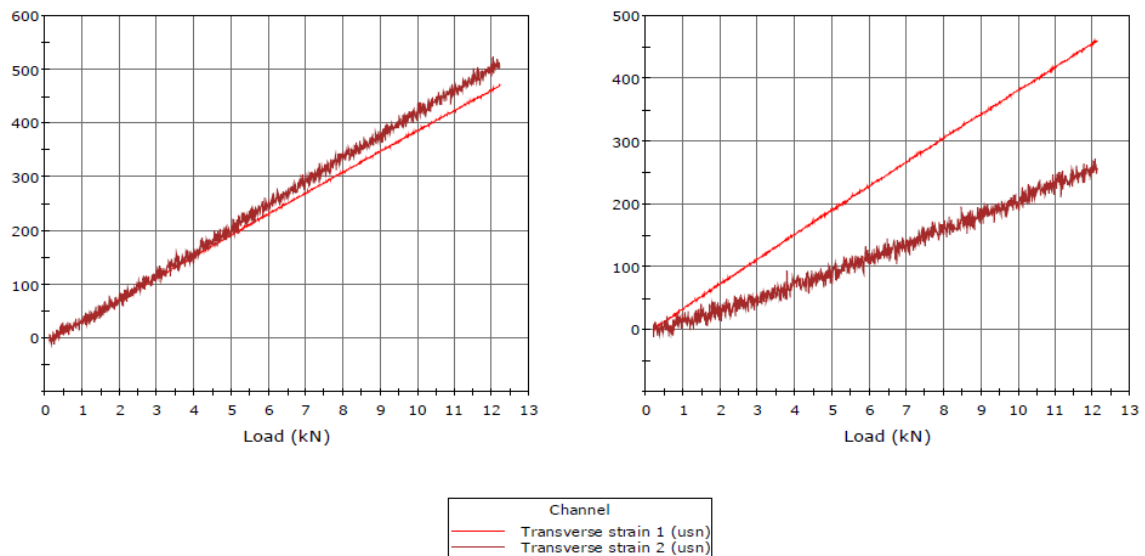


**Figure 4.4: a) First test of transverse extensometer versus transverse strain gage, b) second test with same specimen**

Here “Transverse strain 1” is strain gage and “Transverse strain 2” is extensometer data. While comparing the two graphs, one may notice that strain gage data is very reliable, producing near match results. However extensometer data varies from test to test without having any logical reason. Thus, the providing company changed the extensometer with more reliable, Epsilon 3575 Transverse Averaging extensometer.

#### **4.2. The Investigation of Tensile Behavior of Interply Glass/Carbon Hybrid Composites by Fiber Bragg Gratings**

The number of major published work suggests that research on glass/carbon hybrid composite were most intense between late 1970s and beginning 1990s [7, 22-30]. This fact illustrates that recent advancement in sensor technologies can be utilized in understanding the failure phenomenon of interply hybrid carbon / glass composites. One of the possible candidates to structural sensing of hybrid composite is fiber Bragg gratings.

The literature review shows that ultimate tensile strain of glass and carbon reinforced composite stays within the sensing limits of fiber Bragg gratings. However in

order to monitor FRP specimens under such large deformation, the optical fiber and bulk material interaction described above should be carefully investigated for each fabric type. In the present study, unidirectional carbon fiber and E-glass fabrics with epoxy resin matrix material have been used for hybrid specimen manufacturing. Three set of stacking sequences were investigated by embedded FBG under tensile loading.

#### **4.2.1. Experimental Procedure**

##### **4.2.1.1. Specimen Preparation**

As previously stated in literature review section, there are a number of processing methods for manufacturing composite materials. The one method that is particularly suitable for manufacturing composites with embedded FBG sensors purposes is the vacuum infusion process since it does not require complicated procedure for ingress/egress of optic sensors. With this method, it is possible to produce composites with strength levels that can be achieved with resin transfer molding technique. All of the specimens studied in this section are produced by vacuum infusion method.

The very first step of producing specimens begins with mold surface preparation. This step has 3 sub-steps that are repeated for every composite production. Axel brand cleaner, sealer and release systems are used for surface preparation. Initially, the surface is cleaned by a cleaner to remove off any contaminations such as dust, which may reduce the detachability of composite plate from the surface. When the surface is fully dried, the sealer cycle begins. The sealer is applied to the surface 5 times with 20 minutes intervals with a lint free cloth. After fifth application, it is waited for an hour so that the sealer film is set and gains its mechanical strength. The release is applied to the surface the same way as sealer cycle. These steps ensure that resin does not bond to the mold surface and separate easily. Therefore, they are essential part of the composite production. After the release has been dried for an hour, the reinforcement materials are laid over the surface of the mold.

The second part covers the steps between surface preparation and infusion. Peel ply, flow mesh and bagging material are cut considering the size of reinforcements. The reinforcement material with peel ply and flow mesh is placed on the surface and inlet and outlet tubes are situated so that optimal resin flow is achieved. The sides of bagging

material are covered with sealant putty and then placed on the surface covering the reinforcement. If the reinforcement has embedded fiber optic sensor then hypodermic tube is used to provide the optical cable with a safe exit. To ensure that no leak occurs during the infusion, vacuum is applied to the reinforcement and if necessary additional sealant tape applied to the leaking regions. Infusion part starts with mixing resin and hardener. For all of the experiments described in this thesis, Araldite LY 564 resin and XB3404-1 hardener with 100:36 by weight mix ratio is used as matrix material. While the resin is being mixed, the mold is heated to 45 degrees for lowering the viscosity. Manufacturer's specification states that resin mix can be cured for 8 hours at 80 °C or 15 hours at 50 °C. Therefore to make sure that the composite structure is fully cured, curing has been performed at 70 °C for 15 hours.

As reinforcement materials unidirectional E-glass and Carbon fiber supplied by Metyx, shown in figure 4.5, were used to manufacture specimens. As previously discussed in literature review section, 90° tow perpendicular to the FBG sensor can lead to an uneven strain field on the FBG sensor, hence leading to deterioration in the quality of the FBG spectrum or in the worse case spectrum splitting. In addition as shown in figure 2.1 a composite plate made of unidirectional reinforcements is simpler in terms of understanding the sensor behavior. The properties of E-glass and carbon fiber are given in the table 4.3.

**Table 4.3: Properties of textile reinforcements**

	UD E-Glass Fiber		UD Carbon Fiber	
	0	600 Tex	283 gr/m <sup>2</sup>	800 Tex 12K
90	68 Tex	37 gr/m <sup>2</sup>	68 Tex E-Glass	10 gr/m <sup>2</sup>
Stitch	76 Dtex	10 gr/m <sup>2</sup>	-	-



**Figure 4.5: Reinforcements**

Silica based fiber Bragg gratings were procured from Technicasa and Bragg wavelength of both 1540 nm and 1550 nm with 1 mm grating length. The grating regions are polyamide recoated after FBG writing procedure. The recoating increases the mechanical performance of the FBG sensor. In order to achieve testing goals, few modifications to industry standard ASTM D3039 were performed. First, rectangular shape of specimens narrowed to 20 mm while keeping the length of specimen 250 mm. This enabled the universal test machine to break off the carbon fiber specimens without reaching its ultimate loading limit of 100 kN. Shown in the figure 4.6 an L shaped specimen design was developed so that ingress of optical fiber into the specimen is distant from test zone.

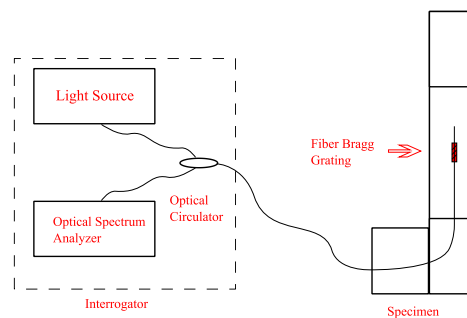


**Figure 4.6: Interrogator and L shaped specimen**

In the figure 4.7 green dashed lines represent L shaped specimen location while the optical fiber route is indicated by red arrows. In order to ensure that during manufacturing stages (i.e. the lay-up, vacuuming and resin infusion), the optical fiber should not be dislocated from its original placement, arranged to be parallel to  $0^\circ$  fiber direction. As shown in the same figure, the FBG sensor is fixed to corresponding ply

through passing it under weaving threads. In addition, due to the carbon fiber reinforcement being optically opaque, the optical fiber has to be fixed adequately otherwise it would be difficult to identify exact location of the optical fiber.

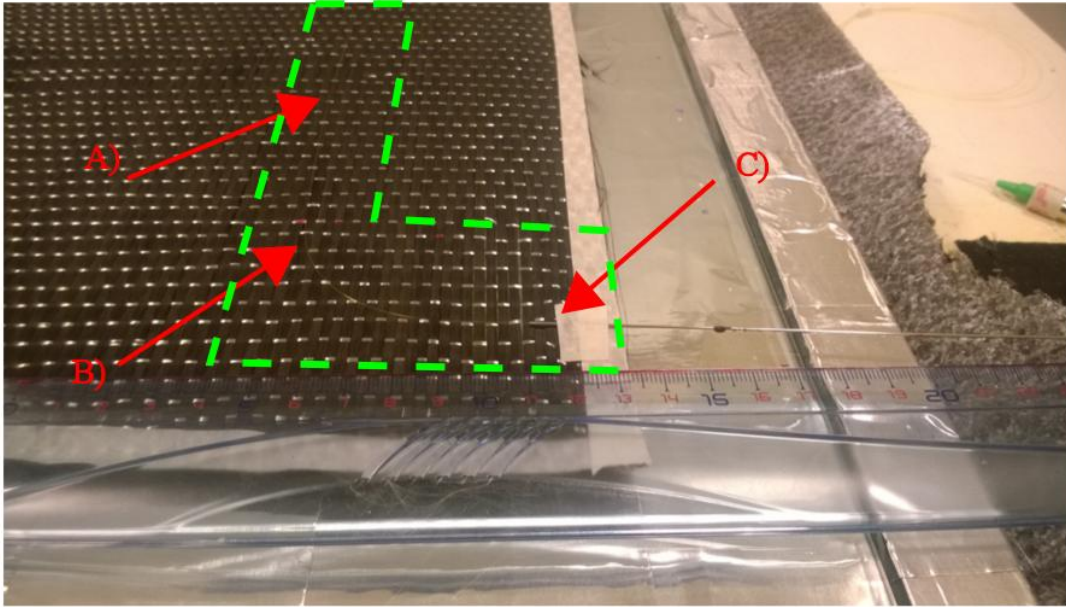


**Figure 4.7: A) FBG location, B) stitched optical fiber, C) optical fiber ingress location**

Three different specimen configurations shown in figure 4.8 were developed for this work. The first two configurations are  $[C_8]$  and  $[G_8]$ . The remaining is the interply hybrid configuration  $[C/G_3]_S$  was formed for 3 different experiments, hybrid 1 – 3. The table 4.4 shows thickness of each specimen. All specimens are prepared in such a way that tensile loading is parallel to  $0^\circ$  axis of every plies. While single fiber type specimens have FBG sensors embedded into neutral axis, all of the hybrid specimens have two FBG sensors, one on the neutral axis and another one at outmost ply. The same figure shows sensor locations, tensile load vector, neutral axis of the specimen and type of the reinforcements. In the figure, green layers are carbon fiber whereas white layers are glass fiber reinforcements. The neutral axis is colored red and the blue mark is the position of FBG sensors. The orange mark shows strain gage location for the corresponding specimens. The black rectangular boxes situated close to corners are tabbing materials. Finally the black arrows indicate the direction of tensile loading.

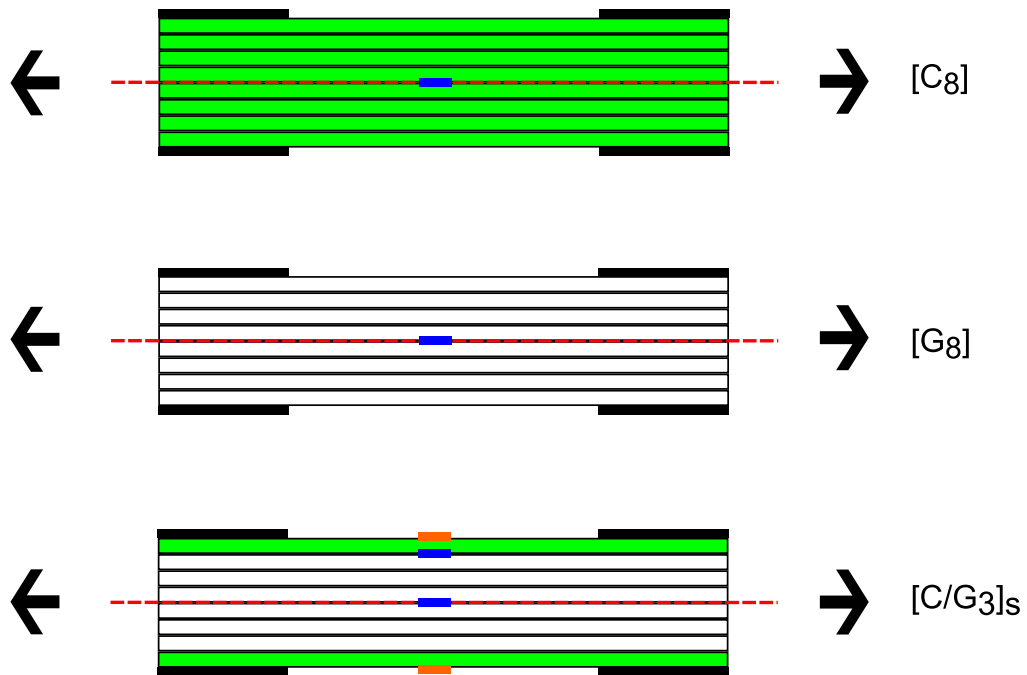


**Figure 4.8: Hybrid stacking sequences, green layers are carbon fiber, white layers are glass fiber reinforcements**

**Table 4.4: Specimen Thickness (mm)**

	Experiment 1	Experiment 2	Experiment 3
Glass Only	2.26	-	-
Carbon Only	2.21	-	-
[C/G <sub>3</sub> ] <sub>s</sub>	2.08	2.22	2.52

A LabVIEW code, shown in Figure 4.9, is developed to acquire strain data from Epsilon 3542 axial extensometer and Vishay PG strain gages.

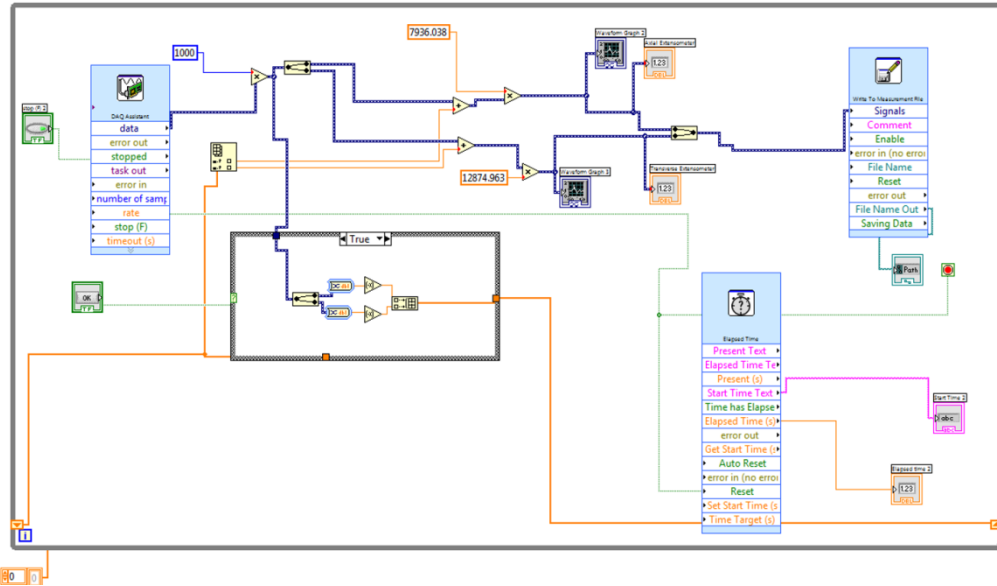


**Figure 4.9: Labview code for extensometer data acquisition**

Zwick Roell Z100 was used in constant speed control mode for testing purposes while National Instruments and Micron Optics systems were used to measure strain and wavelength respectively. During the experiments, data acquisition rate of 1 kHz has been used. The testing setup can be seen in Figure 4.10.

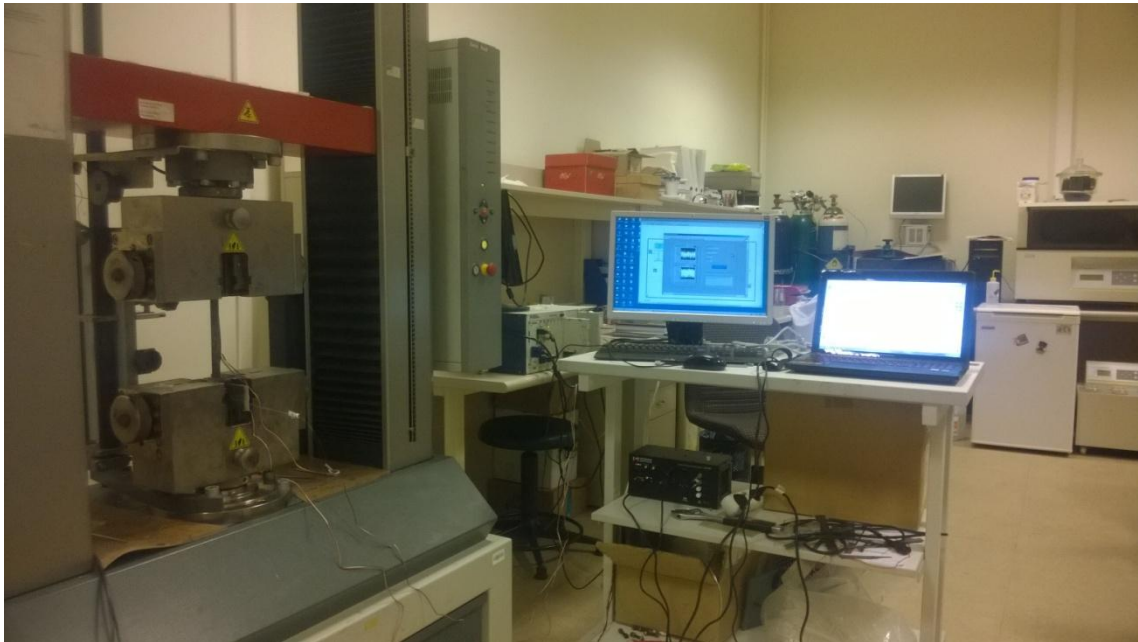


**Figure 4.10: Testing setup**

#### 4.2.1.2. Test Procedure

To be able to monitor the ply splitting of carbon fiber reinforced composites over a longer time interval, several tensile test experiments on carbon reinforced composites without any embedded FBG have been performed with the cross head speed of 2 mm/min whereby the stress level at which first noticeable ply splitting occurs is determined. Specimens with embedded FBG sensors are tested with constant of speed 2 mm/min and then the testing speed is reduced down to 0.2 mm/min upon reaching predetermined stress level causing noticeable ply splitting. Figure 4.13, suggests that reducing extension rate does not affect linearity of the stress versus strain curve. On the other hand, since the glass fiber reinforced composite breaks in a sudden manner, the testing speed was unchanged. Moreover, for many isotropic and orthotropic materials, the testing of specimen stops when the machine detects 40% decrease in the load compared to peak load. However in this case, since the load is expected to drop significantly during progressive failure, the machine is adjusted to stop when the load decrease is beyond 90%. Otherwise the testing stops prematurely without fully breaking off the specimen.

Strain data for test specimens, namely, carbon only, glass only, hybrid 1, and hybrid 2 are collected by using an axial extensometer while for hybrid 3 by using axial strain gages fixed to both sides of the specimen.

#### 4.2.2. Results and Discussion

Initially numerous tests were performed in order to understand macro-mechanical behavior of each specimen configuration. Two successful testing of specimens without embedded FBG sensor were taken into consideration for each manufactured plate. The remaining tests were rejected due to tabbing error and failure modes. The Specimens with outer layer made of carbon fiber were painted with a white color acrylic to detect failure modes. The figure 4.11 shows stress strain behavior of the specimens cut from corresponding composites. The stress strain curves reveal specific properties of composite specimens. The carbon only specimens have the highest ultimate stress whereas glass only specimens have the highest ultimate strain. The failure of carbon only specimen occurs through progressive phase while glass only specimen breaks off

suddenly. On the other hand, the hybrid specimens exhibit progressive failure and hybrid effect. The ultimate strain results of hybrid specimens are considerably higher than carbon only specimens. The figure also reveals that extensometer reading of strain is accurate until first major ply splitting. Since the axial extensometer is attached to the specimen by means of physical contact, any damaged and displaced bundles at contact zone affects accuracy of the extensometer readings.

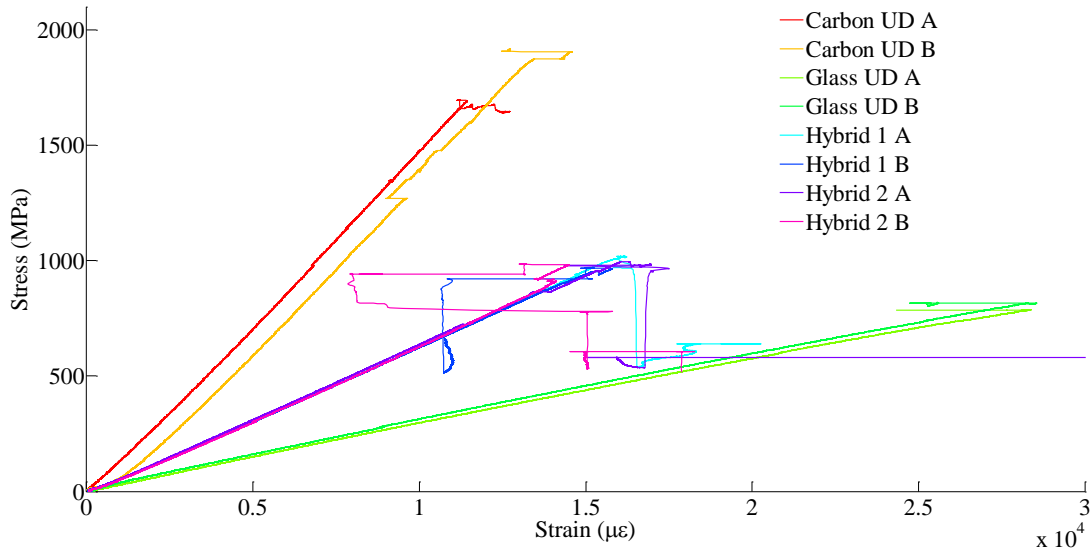


**Figure 4.11: Stress strain curves of neat specimens**

To demonstrate the results efficiently, all of the FBG sensors embedded into carbon fiber ply will be called FBG 1 and FBG2 for the ones embedded into glass fiber ply. Similarly, strain gages in proximity of FBG 1 will be called GAGE 1 whereas the one on the other side will be called GAGE 2. All FBG sensors are calibrated either with respect to the axial extensometer or strain gages to convert wavelength shift into microstrain  $\mu\epsilon$ , and their calibration coefficients are given in the table 4.5. These coefficients are similar to what have been reported in the literature [31, 32].

**Table 4.5: Pm wavelength shift per 1  $\mu\epsilon$  coefficient of specific FBG sensors**

	Carbon Only	Glass Only	Hybrid 1	Hybrid 2	Hybrid 3
FBG 1	1.259	-	1.191	1.191	1.204
FBG 2	-	1.257	1.191	1.191	1.204

A number of topics were investigated using isolation of one parameter at a time method. First, single fiber only specimens were used especially in ultimate strain analysis by FBG sensors. Second, double FBG sensors embedded in interply hybrids were used to reveal the ply by ply behavior of the specimen under tensile loading.

Third, absence of external load (extensometer) and testing anomalies (i.e. bending) were investigated using double strain gages. Last, the comparison of maximum peak wavelength shift was used to study hybrid effect.

Following parts are explained using a nonconventional plotting method due to the fact that signal behavior with respect to synchronized test time shows more detail compared to stress versus strain curves. The stress and strain are plotted with respect to test time by using double Y axis plots. For all plots that have double Y axis, the left hand shows stress while right hand shows strain. Since carbon only, hybrid 1-3 specimens exhibit progressive failure the plots feature close-up curves. The close-up area is marked with dashed rectangles in the original plots. Moreover, in order to monitor the damage progress in hybrid composites under uniaxial tensile testing, the difference between the strain values of FBG 1 and FBG 2 sensors and also strain gages are presented through the help of parameters  $F_x = \varepsilon_c^{fbg} - \varepsilon_g^{fbg}$  and  $S_x = \varepsilon_1^{sg} - \varepsilon_2^{sg}$  where  $\varepsilon_c^{fbg}$  and  $\varepsilon_g^{fbg}$  are the strains recorded by of FBG 1 and FBG 2, respectively and  $\varepsilon_1^{sg}$  and  $\varepsilon_2^{sg}$  strain values of GAGE 1 and GAGE 2. Ideally, for a perfect hybrid laminate, one should expect that both FBG sensors would read the same strain level. However, it should be noted that there are differences between strain values of two FBG sensors. The positive value indicates that FBG 1 is more strained than the FBG 2 while the negative value points to the otherwise. Be reminded that experiments for which results are presented in figure 4.16 and figure 4.17 are performed using axial extensometer and figure 4.18 using strain gages. Similar to stress and strain plots,  $F_x$  plots feature close-up curves covering exact time frame as zoom curves of stress and strain plots.

The single fiber type composite results suggest that the failure of carbon fiber composite occurs in a progressive fashion compared to the glass fiber composite. As expected, ultimate strain of GFRP is much higher while modulus of elasticity and ultimate tensile stress is distinctively lower.

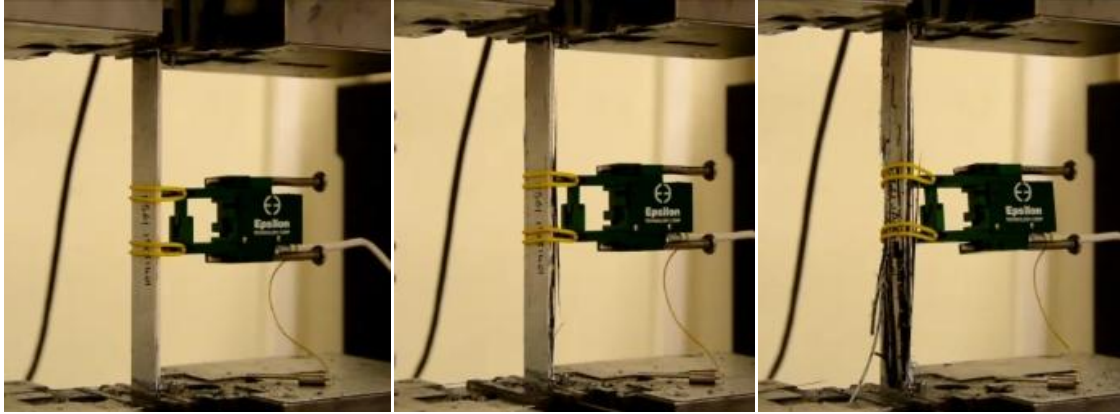


**Figure 4.12: a) undamaged specimen, b) first ply splitting, c) complete failure of carbon fiber plies**

The figure 4.13 shows stress versus strain behavior of CFRP indicating that change of displacement velocity does not affect linearity of the plot. The test speed decreased down to 0.2mm/min at approximately 1500MPa. The figure also reveals that reading of strain is accurate until first major ply splitting. Since the axial extensometer is attached to the specimen by means of physical contact, any damaged and displaced bundles at contact zone affects accuracy of the extensometer readings.

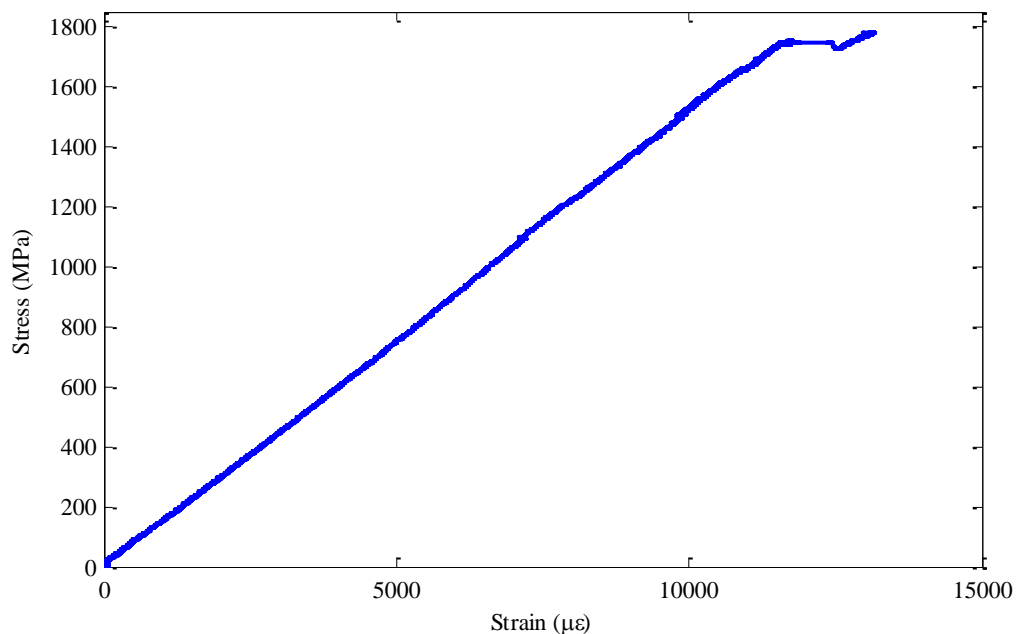


**Figure 4.13: Stress versus strain result of carbon fiber reinforced composite**

The figure 4.14 shows that the FBG sensor is able to sense the strain until last major ply failure. Therefore, it would be a good estimation that fiber bundles around FBG and optical fiber were intact till that point. The multiple sharp declines in the stress

point out the progressive failure in the CFRC, which is also supported by video recording during the experiment. One could note from the figure that the FBG sensor can reliably provide the strain and ply failures accurately. It can be seen from the figure that there is a difference in the strain jumps corresponding to load drops between the FBG sensor and the extensometer, which might be attributed to the fact that the extensometer is attached to the surface and the sudden damage on the fiber bundles pulls extensometer grips more than when the specimen surfaces were intact.

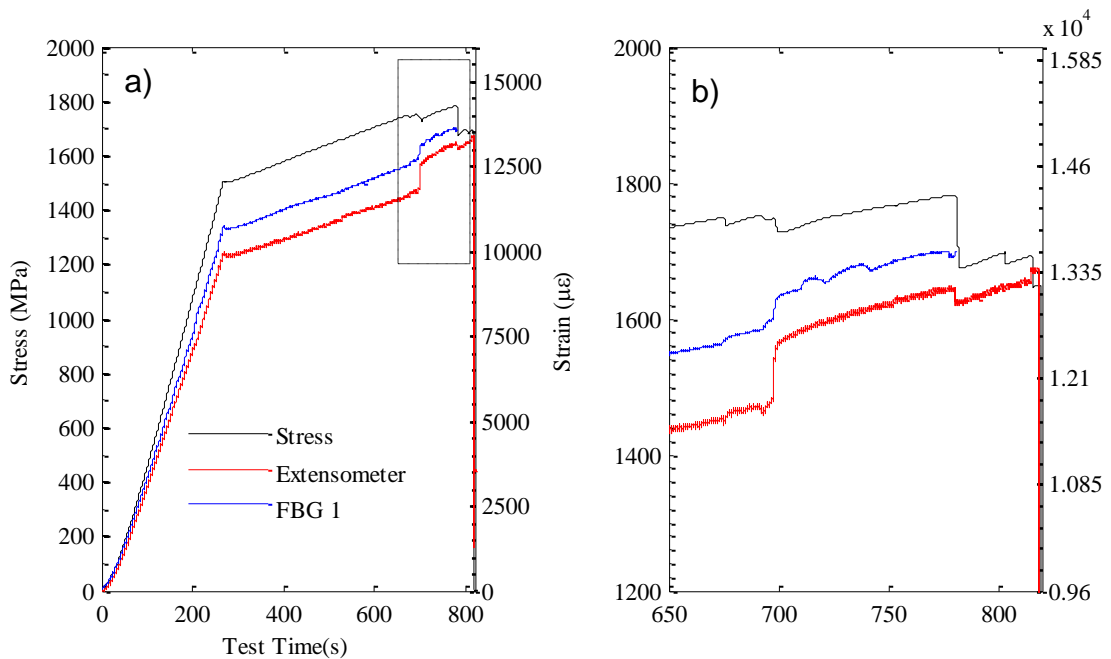


**Figure 4.14: a) Stress and strain curves of carbon only specimen with respect to test time, b) close-up curves**

The failure of GFRC occurs suddenly as can be seen from the figure 4.15. The result shows that silica based FBG sensor can monitor the specimen until ultimate failure. The plot indicates that FBG sensor has good linearity even at such elongations.

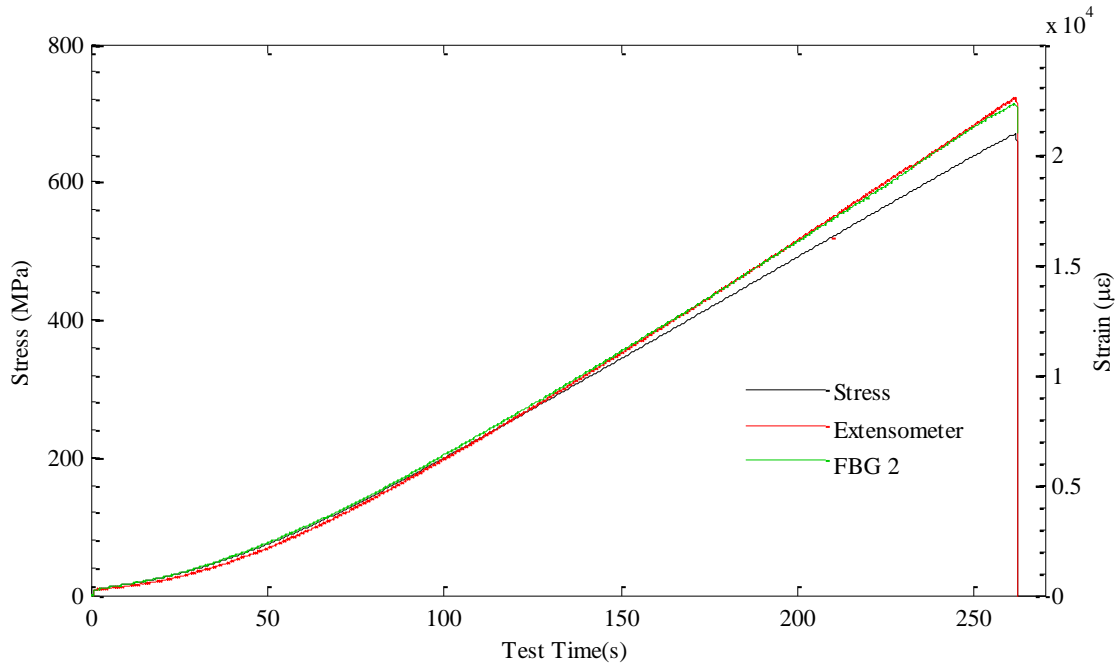


**Figure 4.15: Stress and strain on double Y axis plot of glass fiber reinforced composite**

The hybrid composite 1 result figure 4.16a, shows that FBG sensors at 2 different plies behave macroscopically in a coherent way. In this experiment, FBG sensor embedded into glass fiber ply failed to send signal earlier than the one embedded into carbon fiber ply, which is not expected referring to the strain range given in the figure 4.15 the FBG sensor is able to withstand. This suggests that either optical fiber failed early due to a defect or a matrix crack around the optical fiber led to failure of the optical fiber. On the other hand FBG sensor at carbon fiber ply was active until last major ply failure.

The random sinusoidal like variation shown in figure 4.16c, are deemed to be due to the vibration induced bending on the specimens by the presence of the extensometer. The sudden discrete variation corresponds to the steps in the stress as given figure 4.16a. The rise in the strain variation indicates that glass fiber is failing and the carbon fiber starts to take the load. This conclusion can also be visualized in figure 4.17.

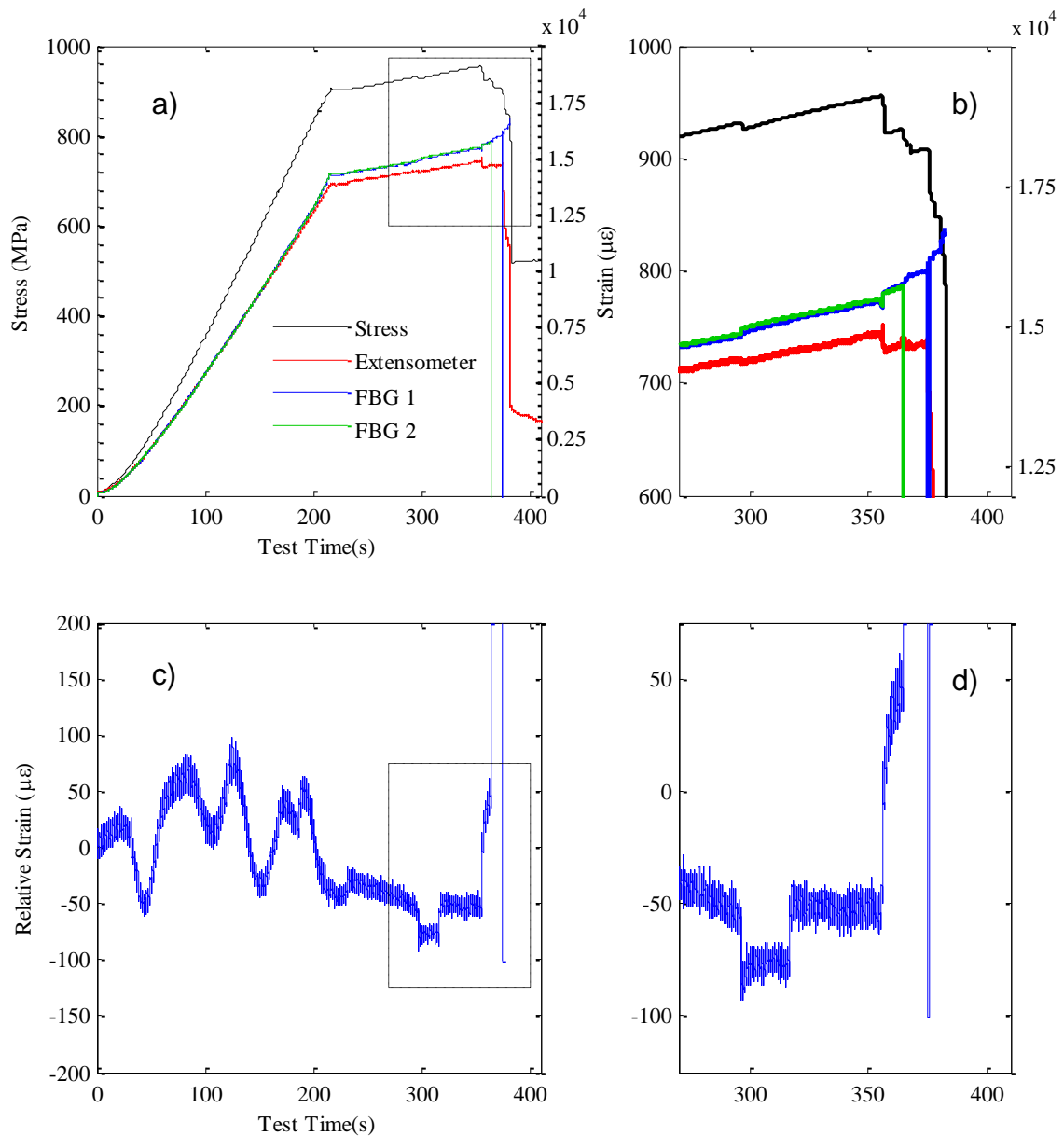


**Figure 4.16: a) stress and strain curves of hybrid 1, b) close-up curve, the location is demonstrated by dashed rectangle, c) Fx curve of hybrid 1, d) close-up Fx curve**

The hybrid composite 2 result, figure 4.17, is similar to the hybrid 1. Moreover, both FBG sensors were able to send signals until last major ply split at carbon fiber plies. During that major failure it is observed that one of the peaks were alive on the spectrum screen when last major failure occurred. However, the peak tracking algorithm of the interrogator software couldn't detect it. It is suspected that due to the sudden load transfer, large shift of peak wavelength caused tracking algorithm to miss the peak entirely.

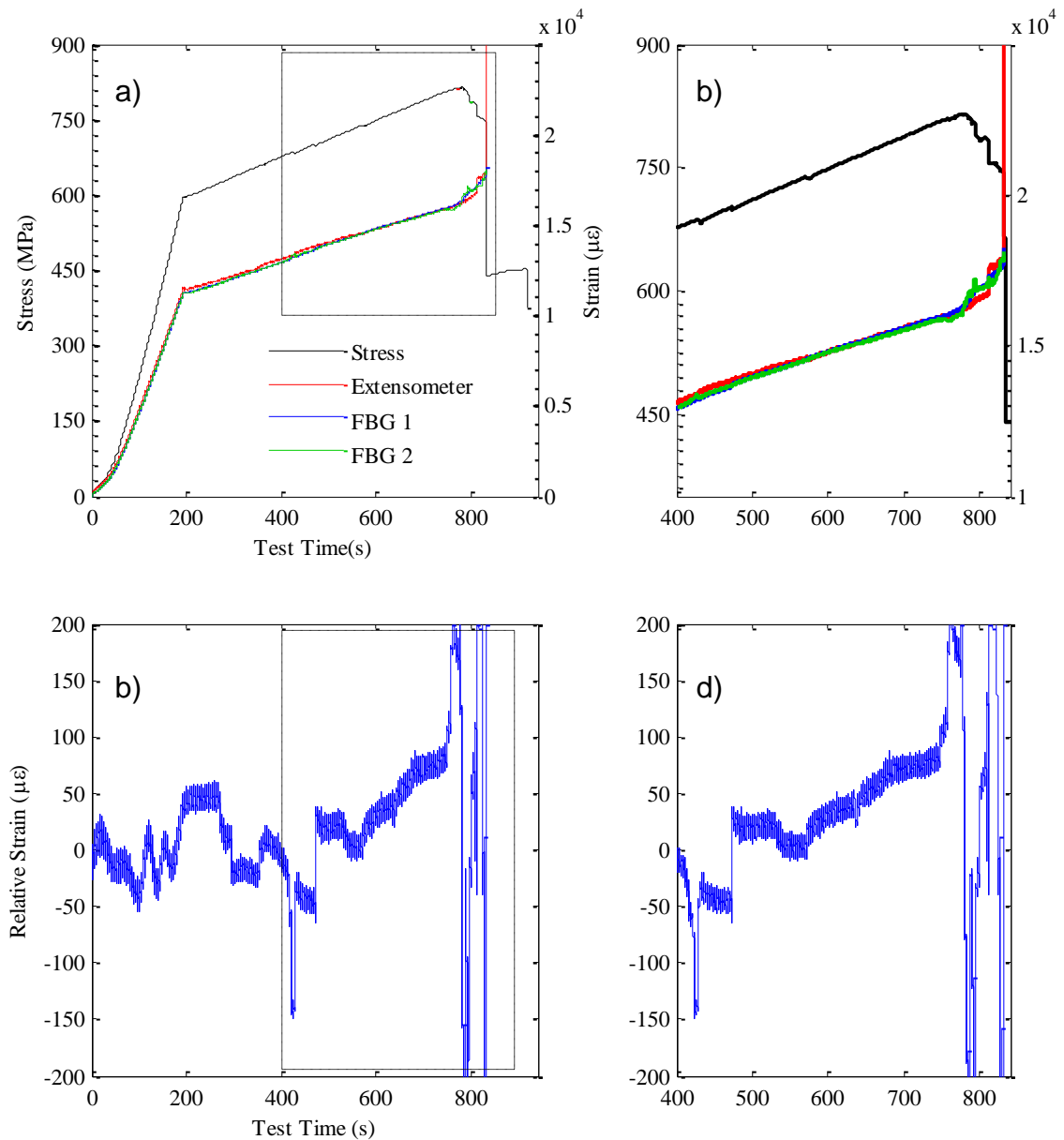


**Figure 4.17: a) stress and strain curves of hybrid 2, b) close-up curve, c) Fx curve of hybrid 2, d) close-up Fx curve**

The hybrid composite 3 test utilized two strain gages bonded axially to the both sides of specimen. The result in figure 4.18a, shows that strain gages are susceptible to large deformations. In this test, failure of peak tracking was more frequent that resultant graph has several data gaps. The remaining data recovered by resetting the peak tracking algorithm in the middle of experiment which cost between 20000 to 40000 data points. This result also shows that after last major failure at carbon fiber plies the fiber optics were still intact. As expected FBG sensor embedded into glass fiber ply continued to capture strain while the one embedded into carbon fiber ply shows almost

no strain compared to initial position. Both of FBG sensors were active until ultimate failure. To be able to substantiate whether the random sinusoidal like variation in strain up to 200 seconds is due to the extensometer induced bending, this experiment is repeated without extensometer and strains are monitored with strain gages attached to the both surface of the specimen such that they are aligned with the location of embedded FBGs. It is a common practice to attach uniaxial strain gages to both surfaces of the specimen to measure bending strain in cantilever beam. During the testing of hybrid 3, both of the strain gages were debonded from the surface at approximately 11000 microstrains.

The relatively flat horizontal behavior of  $S_x$  in figure 4.18c shows that the specimen is not subjected to bending during the testing and the FBG strain variation no longer bears resemblance to random sinusoidal form. It can be noted from the figure that there are strain variations between FBG sensors that strain gages are not able to capture. The sudden discrete drops in strain variance in this case also follows the trend in the corresponding stress values, which indicates the effectiveness of FBG sensors for monitoring ply failure. Moreover for quasistatic loading scenarios, variations of 100 microstrains may not affect the overall results however, in fatigue testing where load cycles can reach to the level of several millions, this variation may indeed affect the fatigue life of the composite.

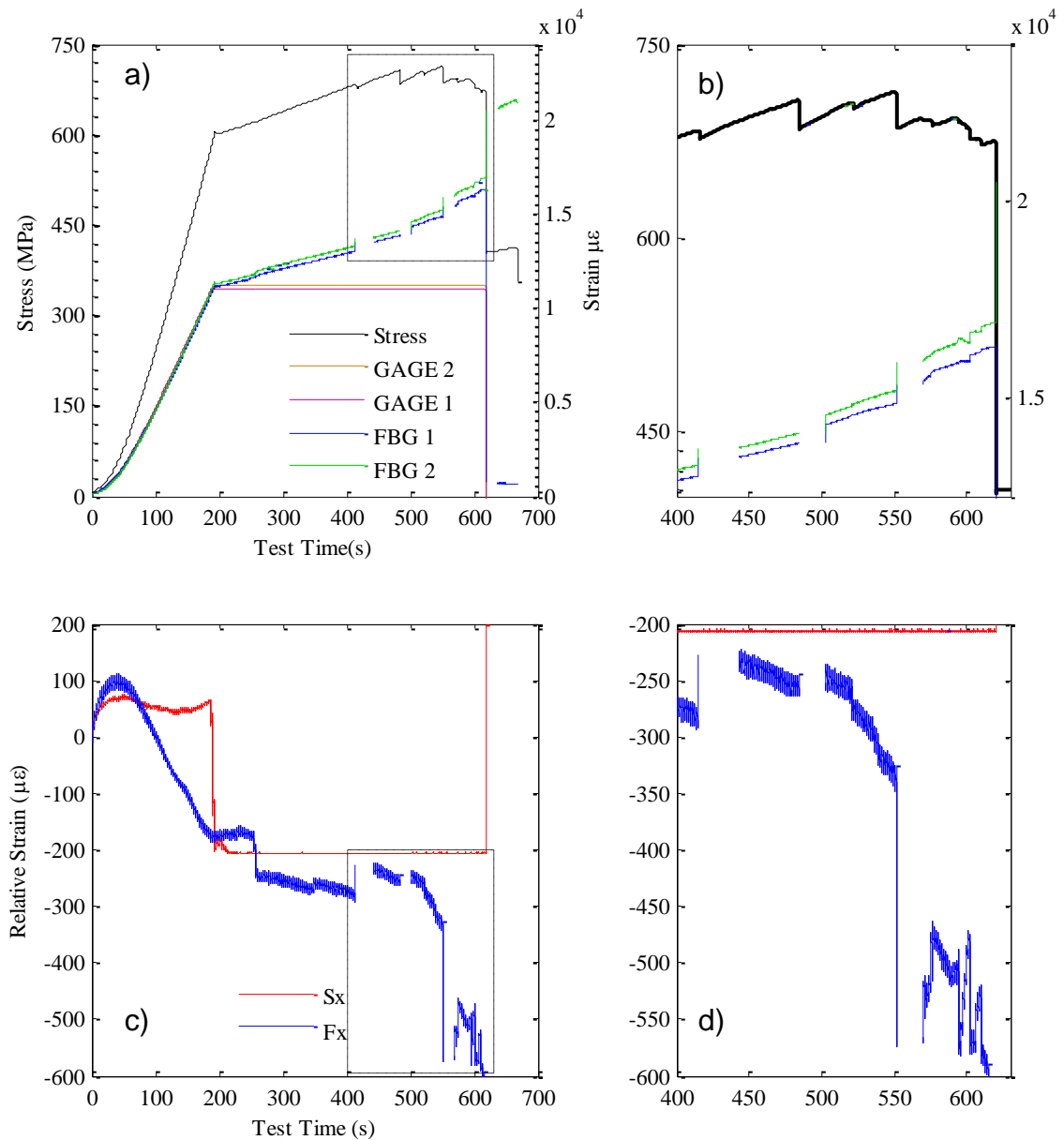


**Figure 4.18: a) stress and strain curves of hybrid 1, b) close-up curve, c)  $F_x$  and  $S_x$  curves of hybrid 3, d) close-up  $F_x$  and  $S_x$  curve**

The maximum amounts of FBG wavelength shift per FBG sensor are tabulated in table 4.6. The hybrid effect which is demonstrated in literature review and neat specimen results in figure 4.11, is noticeable from the recorded wavelength shifts. At this point be reminded that the hybrid effect is the extension of ultimate strain of low elongation fiber when hybridized with high elongation fiber. The single fiber type specimens exhibit lowest and highest wavelength shift whereas FBG sensors in hybrid specimens have few nanometers more shift compared to FBG sensor in carbon fiber only composite. Moreover, the 28.07 nm wavelength shift captured at ultimate tensile

strain of glass fiber composite is one of the highest ever tracked on silica based FBG sensor. This suggests that surrounding the optical fiber with load carrying fibers and the matrix and the minimal transversal load increases the ultimate tensile strain of FBG sensor.

**Table 4.6: Maximum recorded wavelength shift (nm) per specimen**

	Carbon Composite	Glass Composite	Hybrid Composite 1.1	Hybrid Composite 1.2	Hybrid Composite 1.3
FBG 1	16.33	-	19.98	21.71	19.65
FBG 2	-	28.07	18.74	21.59	25.27

## CHAPTER 5

### Conclusion

Within the scope of this thesis, two of the major fiber reinforced composite manufacturing methods developed; manufactured interply hybrid specimens are monitored under tensile loading by embedded fiber Bragg gratings and a new laboratory that is capable of fatigue analysis of composites built at Yonca-Onuk Company. At first one may not notice the connection between these three distinct topics. On the contrary, in order to monitor the structure there has to be efficient solution for embedding the sensor. Moreover, without the sound knowledge of the structure, the sensor output implies very little information.

The challenge of structural health monitoring of composites by embedded FBG sensors starts with developing necessary composite manufacturing method. During this thesis work, it is found that fiber optic placement and reliability of composite specimen play crucial roles in overall system design. Hence, a novel resin transfer molding and vacuum infusion units focusing different areas of structural health monitoring are developed. Compared to the preceding unit, the new RTM system has many useful features. The most important ones are the following: better overall lifetime, better specimen accuracy, efficient heating, calculated ergonomics. On the course of completing the RTM design, the most challenging topic worth mentioning was the optimization of design quality without affecting the manufacturing costs.

Intensive literature review shows that carbon/glass hybridization is a well researched area. There are numerous benefits reported both in industry and academia. On the other hand, FBG sensor technology is already utilized in many applications such as structural health monitoring. In this work it is shown that interply hybrid composites can benefit from embedded FBG sensors. The embedded sensors were able to track failure behavior of the specimens under quasistatic tensile loading. The working

wavelength range of FBG sensor embedded into glass fiber reinforced composite is one of the highest compared to reported studies. Moreover, repetitive results of 20nm wavelength shift are obtained from interply hybrid specimens.

Further studies on interply hybrid composites should include many widely used reinforcements. The mechanics of the material type coupled with weave patterns affects the output of embedded sensors.

## References

1. Anon, *Application of carbon fibre ribbon*. Composites, 1972. **3**(4): p. 148.
2. Anon, *Carbon fibre helps create powerboat records*. Reinforced Plastics, 1973. **17**(1): p. 7.
3. *HexPly Prepreg Technology*. Hexcel Corp.
4. Jang, B.-W., et al., *A health management algorithm for composite train carbody based on FEM/FBG hybrid method*. Composite Structures, 2010. **92**(4): p. 1019-1026.
5. Phillips, L.N., *Improving racing-car bodies*. Composites, 1969. **1**(1): p. 50-51.
6. Hayashi T. *On the improvement of mechanical properties of composites by hybrid composition*. in *8th International Reinforced Plastics Conference*. 1972. Brighton: British Plastics Federation.
7. Bunsell, A.R. and B. Harris, *Hybrid carbon and glass fibre composites*. Composites, 1974: p. 157-164.
8. Hill, K.O., et al., *Photosensitivity in optical waveguides: Application to reflection filter fabrication*. Appl. Phys. Lett., 1978. **32**(10): p. 647.
9. Meltz, G., W.W. Morey, and W.H. Glenn, *Formation of Bragg gratings in optical fibres by transverse holographic method*. Opt. Lett., 1989. **14**(15): p. 823.
10. Tao, X.M., et al., *Internal Strain Measurement by Fiber Bragg Grating Sensors in Textile Composites*. Composites Science and Technology, 2000. **60**: p. 657-669.
11. Kuang, K.S.C., et al., *Embedded Fiber Bragg Grating Sensors in Advanced Composite Materials*. Composites Science and Technology, 2001. **61**: p. 1373-1387.
12. Lu, C., et al., *Impact of Embedding Techniques on FBG Sensors*. 2004.

13. Fraden, J., *Handbook of Modern Sensors: Physics, Designs, and Applications*. 4th ed. 2010: Springer.
14. Kang, D.H., et al., *The signal characteristics of reflected spectra of fiber Bragg grating sensors with strain gradients and grating lengths*. NDT & E International, 2005. **38**(8): p. 712-718.
15. Kang, D.H., et al., *Mechanical Strength Characteristics of Fiber Bragg Gratings Considering Fabrication Process and Reflectivity*. Journal of Intelligent Material Systems and Structures, 2006. **18**(4): p. 303-309.
16. Skontorp, A. *Strength and failure mechanisms of polyimide-coated optical fibers*. in *Smart Structures and Materials 2000: Sensory Phenomena and Measurement Instrumentation for Smart Structures and Materials*. 2000. SPIE.
17. Yoon, H.-J. and C.-G. Kim, *The mechanical strength of fiber Bragg gratings under controlled UV laser conditions*. Smart Materials and Structures, 2007. **16**(4): p. 1315-1319.
18. *Guide to Composites*, G. Inc., Editor.
19. *Technical Design Guide for FRP Composite Products and Parts*, M.F.G.C. Corp., Editor.
20. Dictionaries, O., "prepreg". *Oxford Dictionaries*. Oxford University Press.
21. *Carbon and low alloy steel St52-3 steel plate*, H.B.i.c. Ltd., Editor.
22. Zweben, C., *Tensile strength of hybrid composites*. Journal of Materials Science, 1977. **12**: p. 1325-1337.
23. Summerscales, J. and D. Short, *Carbon fibre and glass fibre hybrid reinforced plastics*. Composites Part A: Applied Science and Manufacturing, 1978: p. 157-166.
24. Manders, P.W. and M.G. Bader, *The strength of hybrid glass/carbon fibre composites: Part 1 Failure strain enhancement and failure mode*. Journal of Materials Science, 1981. **16**: p. 2233-2245.
25. Ni, R.G., D.X. Lin, and R.D. Adams, *The dynamic properties of carbon-glass fibre sandwich-laminated composites: theoretical, experimental and economic considerations*. Composites, 1984. **15**(4): p. 297-304.
26. Kretsis, G., *A review of the tensile, compressive, flexural and shear properties of hybrid fibre-reinforced plastics*. Composites, 1987. **18**(1): p. 13-23.

27. Takahashi, K. and T.-W. Chou, *Non-linear deformation and failure behaviour of carbon/glass hybrid laminates*. Journal of Composite Materials, 1987. **21**(1): p. 396-420.
28. Gutans, J. and V. Tamuzs, *Strength probability of unidirectional hybrid composites*. Theoretical and Applied Fracture Mechanics, 1987. **7**(3): p. 193-200.
29. Zeng, Q.-D., F.-Q. Fan, and Y.-Y. Zhang, *A random critical-core theory of microdamage in interply hybrid composites: I—First failure and hybrid effect*. Composites Science and Technology, 1993. **49**(4): p. 341-348.
30. Zeng, Q.-D., L. Ling, and Z.-L. Wang, *Statistical Strength of unidirectional composites and the effect of interfacial shear strength*. Composites Science and Technology, 1996. **56**: p. 1191-1200.
31. *Optical Fiber Sensors Guide*. 2013, Micron Optics Inc.
32. Othonos, A. and K. Kalli, *Fiber Bragg Gratings: Fundamentals and Applications in Telecommunications and Sensing*. 1999: Artech House.
33. Simonsen, H.D., R. Paetsch, and J.R. Dunphy, *Fiber Bragg grating sensor demonstration in glass-fiber reinforced polyester composite*. First European Conference on Smart Structures and Materials, ed. B. Culshaw, P.T. Gardiner, and A.M. McDonach. Vol. 1777. 1992, Bristol: Iop Publishing Ltd. 73-76.
34. Bullock, D., J. Dunphy, and G. Hufstetler, *Embedded Bragg grating fiber optic sensor for composite flexbeams*. Fiber Optic Smart Structures and Skins V, ed. R.O. Claus and R.S. Rogowski. Vol. 1798. 1993, Bellingham: Spie - Int Soc Optical Engineering. 253-261.
35. Du, W., et al., *Fundamentals and Applications of Optical Fiber Bragg Grating Sensors to Textile Structural Composites*. Composite Structures, 1998. **42**: p. 217-229.
36. Tsuda, H., N. Toyama, and J. Takatsubo, *Damage Detection of CFRP Using Fiber Bragg Gratings*. Journal of Materials Science, 2004. **39**: p. 2211-2214.
37. Botsis, J., et al., *Embedded fiber Bragg grating sensor for internal strain measurements in polymeric materials*. Optics and Lasers in Engineering, 2005. **43**(3-5): p. 491-510.
38. Takeda, N., et al., *Development of smart composite structures with small-diameter fiber Bragg grating sensors for damage detection: Quantitative evaluation of delamination length in CFRP laminates using Lamb wave sensing*. Composites Science and Technology, 2005. **65**(15-16): p. 2575-2587.

39. Sekine, H., et al., *Structural Health Monitoring of Cracked Aircraft Panels Repaired with Bonded Patches Using Fiber Bragg Grating Sensors*. Applied Composite Materials, 2006. **13**(2): p. 87-98.
40. Wang, Y., et al., *Integrated Measurement Technique for Curing Process-Dependent Mechanical Properties of Polymeric Materials Using Fiber Bragg Grating*. Experimental Mechanics, 2007. **48**(1): p. 107-117.
41. Suresh, R., S.C. Tjin, and S. Bhalla, *Multi-component force measurement using embedded fiber Bragg grating*. Optics & Laser Technology, 2009. **41**(4): p. 431-440.
42. Silva-Muñoz, R.A. and R.A. Lopez-Anido, *Structural health monitoring of marine composite structural joints using embedded fiber Bragg grating strain sensors*. Composite Structures, 2009. **89**(2): p. 224-234.
43. Panopoulou, A., et al., *Dynamic fiber Bragg gratings based health monitoring system of composite aerospace structures*. Acta Astronautica, 2011. **69**(7-8): p. 445-457.
44. Moslehi, B., R.J. Black, and F. Faridian, *Multifunctional Fiber Bragg Grating Sensing System for Load Monitoring of Composite Wings*. 2011.
45. Papantoniou, A., G. Rigas, and N.D. Alexopoulos, *Assessment of the strain monitoring reliability of fiber Bragg grating sensor (FBGs) in advanced composite structures*. Composite Structures, 2011. **93**(9): p. 2163-2172.
46. Luyckx, G., et al., *Strain measurements of composite laminates with embedded fibre bragg gratings: criticism and opportunities for research*. Sensors (Basel), 2011. **11**(1): p. 384-408.
47. Schizas, C., et al., *Monitoring of non-homogeneous strains in composites with embedded wavelength multiplexed fiber Bragg gratings: A methodological study*. Composite Structures, 2012. **94**(3): p. 987-994.
48. Ramly, R., W. Kuntjoro, and M.K.A. Rahman, *Using Embedded Fiber Bragg Grating (FBG) Sensors in Smart Aircraft Structure Materials*. Procedia Engineering, 2012. **41**: p. 600-606.
49. Davis, C., et al., *High-strain fiber bragg gratings for structural fatigue testing of military aircraft*. Photonic Sensors, 2012. **2**(3): p. 215-224.
50. Zhu, X.Y., Z.X. Li, and Y.X. Jin, *Laminar fracture behaviour of (carbon/glass) hybrid fibre reinforced laminates—I. Laminar fracture process*. Engineering Fracture Mechanics, 1993. **44**(4): p. 545-552.

51. Zeng, Q.-D., *A random critical-core theory of microdamage in interply hybrid composites: II—ultimate failure*. Composites Science and Technology, 1994. **52**(4): p. 481-487.
52. Harlow, D.G., *Statistical properties of hybrid composites: asymptotic distributions for strain*. Reliability Engineering and System Safety, 1997. **56**: p. 197-208.
53. Hwang, S.-F. and C.-P. Mao, *Failure of delaminated interply hybrid composite plates under compression*. Composites Science and Technology, 2001. **61**: p. 1513-1527.
54. Wu, Z., et al., *Tensile fatigue behaviour of FRP and hybrid FRP sheets*. Composites Part B: Engineering, 2010. **41**(5): p. 396-402.
55. Hai, N.D., et al., *Structural behavior of hybrid FRP composite I-beam*. Construction and Building Materials, 2010. **24**(6): p. 956-969.
56. Dong, C. and I.J. Davies, *Optimal design for the flexural behaviour of glass and carbon fibre reinforced polymer hybrid composites*. Materials & Design, 2012. **37**: p. 450-457.
57. N, G.M., *Hybrid Effects on Tensile Properties of Carbon/Glass Angle Ply Composites*. Advances in Materials, 2013. **2**(3): p. 36.
58. Dai, G. and L. Mishnaevsky, *Fatigue of hybrid glass/carbon composites: 3D computational studies*. Composites Science and Technology, 2014. **94**: p. 71-79.
59. Rana, S., et al., *Development of hybrid braided composite rods for reinforcement and health monitoring of structures*. ScientificWorldJournal, 2014. **2014**: p. 170187.
60. Dong, C. and I.J. Davies, *Flexural and tensile moduli of unidirectional hybrid epoxy composites reinforced by S-2 glass and T700S carbon fibres*. Materials & Design, 2014. **54**: p. 893-899.
61. Mishnaevsky, L. and G. Dai, *Hybrid carbon/glass fiber composites: Micromechanical analysis of structure–damage resistance relationships*. Computational Materials Science, 2014. **81**: p. 630-640.
62. Swolfs, Y., et al., *Tensile behaviour of intralayer hybrid composites of carbon fibre and self-reinforced polypropylene*. Composites Part A: Applied Science and Manufacturing, 2014. **59**: p. 78-84.
63. Sathishkumar, T., J. Naveen, and S. Satheeshkumar, *Hybrid fiber reinforced polymer composites - a review*. Journal of Reinforced Plastics and Composites, 2014. **33**(5): p. 454-471.